VEÐURSTOFA ÍSLANDS

Report
08003

Tómas Jóhannesson
Kristín Martha Hákonardóttir, VST
Carl B. Harbitz, NGI
Ulrik Domaas, NGI

Background for the determination of dam height in the SATSIE dam design guidelines

VÍ-VS-02
Reykjavík
March 2008

Report - Greinargerð
08003

Tómas Jóhannesson
Kristín Martha Hákonardóttir[1]
Carl B. Harbitz[2]
Ulrik Domaas[2]
[1]VST Consulting Engineers Ltd.
[2]Norwegian Geotechnical Institute

Background for the determination of dam height in the SATSIE dam design guidelines

VÍ-VS-02
Reykjavík
March 2008

Contents

List of Tables

List of Figures

1 Introduction

A substantial improvement in the understanding of the flow of snow avalanches against dams and other obstructions has taken place over the last 5–10 years. This improved understanding has been achieved by theoretical analyses, chute experiments, numerical simulations with a new generation of 2D depth-averaged snow avalanche models, and an interpretation of flow marks of snow avalanches that have hit man-made dams and natural obstructions. This development makes it possible to formulate improved design criteria for catching and deflecting dams based on more advanced dynamic concepts, which solve some of the inconsistencies that are associated with the traditional criteria for the design of such dams. In spite of this progress, understanding of the dynamics of the impact of snow avalanches with obstacles remains incomplete, so that some subjective and partly justified concepts are needed in the formulation of the new criteria.

This report is intended as background for the formulation of dam design criteria that are the main content of the SATSIE dam design guidelines/handbook. It is based on discussions within the SATSIE handbook writing group and on discussions of the group with other scientists in this field. The report contains suggested formulae for the computation of dam height based on terrain conditions, dam geometry and the velocity and flow depth of the chosen design avalanche at the location of the dam. Some dynamic background for the formulae is also given. References are made to reports and papers that have been produced within and outside of SATSIE, but these are not summarised here so that the reader needs to consult these original sources for more detailed information.

The traditional design criteria for catching and deflecting dams are based on viewing the avalanche as a point-mass. As a consequence of this simplification, lateral and longitudinal interactions between different parts of the avalanche are ignored. Point-mass trajectories corresponding to different lateral parts of an avalanche that is deflected by a deflecting dam must intersect as already deflected material on its way down the dam side collides with material heading towards the dam farther downstream. Similarly, it is clearly not realistic to consider the flow of snow in the interior of an avalanche that hits a catching dam without taking into account the snow near the front that has already been stopped by the dam. The effect of this interaction on the run-up cannot be studied based on point-mass considerations, and a more complete physical description of lateral and longitudinal interactions within the avalanche body during impact with an obstacle must be developed. The simplest such description is based on a depth-averaged formulation of the dynamic equations for the flow of a thin layer of granular material down inclined terrain. This description is intended to represent the dynamics of the dense core of a snow avalanche, but the saltation and powder components of the avalanche are neglected.

The depth-averaged formulation cannot represent some processes that may be important in the flow of snow avalanches against obstacles. Among such processes are splashing during the initial impact (see Hákonardóttir and Hogg, 2005), overflow of the saltation and powder components, and the transfer of snow from the dense core into suspension during the impact. Processes related to two-phase dynamics and air pressure in the interstitial air in the avalanche that may cause “hydroplaning” or “aeroplaning”, may also be important during overflow, as well as shearing flow over the dam, where a thick avalanche overflows a dam over a part of the flow depth. These aspects of the dynamics will not be considered here.

2 Background

Terrain slope at the dam location in the direction of steepest descent is denoted by ψ and the slope of the terrain normal to the dam axis by $\psi_\perp$. The (dense core of the) design avalanche has flow depth h_1 and depth-averaged velocity u_1 at the dam location (that is directly upstream of the dam before the dam has any effect on the flow) (see Fig. 1). The shape of the terrain and the avalanche flow upstream of the dam are assumed to be sufficiently uniform that spatial variations in ψ, u_1 and h_1 may be ignored. A sloping coordinate system is aligned with the terrain upstream of the dam with the x-axis along the flow direction, which is assumed to be directly in the downslope direction. The y-axis points away from the dam, and the z-axis points upwards in a direction normal to the terrain (see Fig. 2). The deflecting angle of the dam is denoted by φ and the angle between the upper dam side and the terrain, in the direction normal to the dam axis, is α. The snow depth on the terrain, h_s, is not explicitly considered in the following discussion and simply added in the end, assuming that h_s is sufficiently uniform in space that this is appropriate.

Flow depth, dam height and run-up on the dam side are here defined in the direction normal to the terrain upstream of the dam. Vertical dam height and vertical run-up will in general be slightly different from the corresponding heights measured normal to the terrain. Since protection dams are typically built in the run-out areas of avalanches where terrain slopes are small, this difference is not considered explicitly below, and all quantities are expressed in a coordinate system that is aligned with the terrain (see Fig. 2). When dam heights have been determined according to the method outlined below, the corresponding vertical dimensions may be determined from geometrical expressions that transform dimensions normal to the terrain to vertical dimensions.

The run-up of the avalanche on the dam is sometimes written as $h_r = h_u + h_1$, where h_u is run-up corresponding to the velocity of the avalanche and h_1 is the upstream flow depth. Here, it is more convenient to consider the combined run-up, h_r, rather than the components

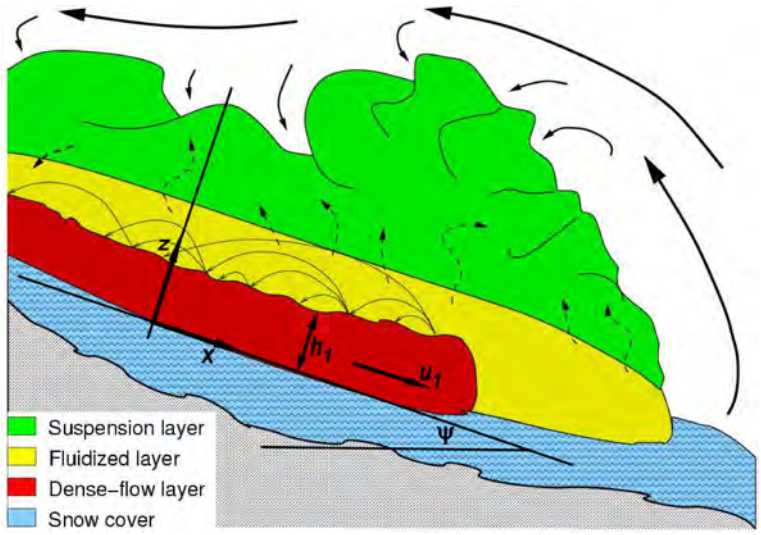

Figure 1: Schematic figure of a dry-snow avalanche showing the dense core, the fluidised (saltation) layer and the powder cloud. The depth-averaged quantities u_1 and h_1 apply to the dense core in the sloping x,z-coordinate system. The figure is adapted from Issler (2003).

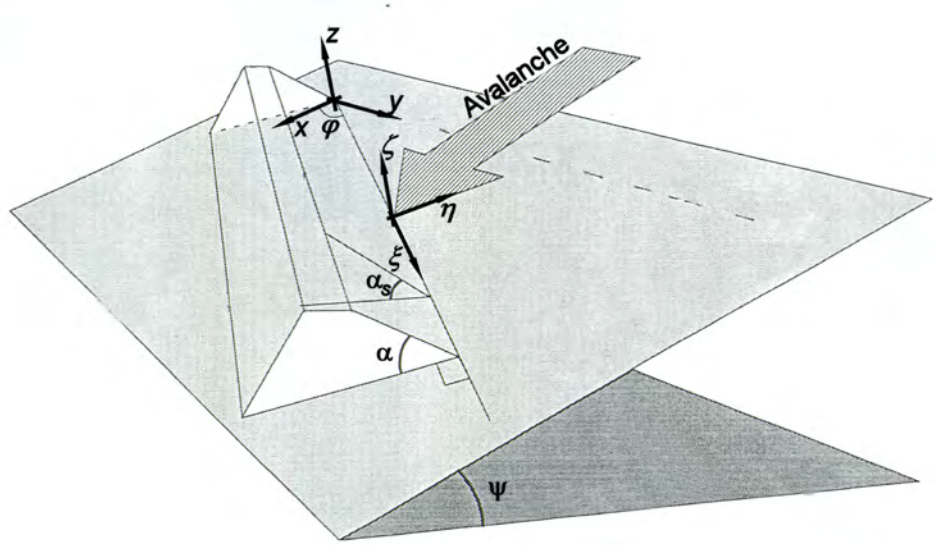

Figure 2: Schematic figure of a deflecting dam showing the x,y,z- and ξ,η,ζ-coordinate systems, the deflecting angle, φ, the slope of the terrain, ψ, and the angle between the upper dam side and the terrain, α. The figure is adapted from Domaas and Harbitz (1998).

h_u and h_1.

Frictional forces are not considered explicitly in the analysis. However, they are implicitly assumed to balance the downslope component of gravity so that the oncoming flow can be assumed to be non-accelerating and spatially uniform. The role of terrain friction in the dynamics of an impact of an avalanche with a dam is not well understood, as evidenced by the fact that the Coulomb friction coefficient μ appears in some expressions for the design height of dams but not in others. However, one may expect terrain friction to be comparatively unimportant in the impact of dry-snow avalanches with dams. For each part of the avalanche body, the impact does not last long enough for frictional forces to reduce the momentum of the avalanche significantly. In addition, many dams are located in gently sloping terrain, where friction is partially balanced by downslope gravity. Assuming that frictional forces are approximately balanced by downslope gravity may not be realistic in some situations, in particular for long deflecting dams with acute deflecting angles, where the deflecting process lasts relatively long for each part of the avalanche body. An analysis of the simplified situation without friction, does, however, lead to valuable insight into the dynamics of the impact with a dam. The simplified results may also be expected to provide an upper bound for design dam height even when friction cannot be neglected.

Entrainment of snow from the snow cover into the avalanche or deposition of snow from the avalanche onto the terrain is also neglected here. These are poorly understood processes that may affect avalanche–dam interactions to some degree. In particular, deposition may be an important process under some circumstances where a part of the avalanche may pile up in front of a dam and form a platform over which the remainder of the avalanche may flow and overtop the dam. This aspect of avalanche–dam interactions will, however, not be further considered in the analysis below.

Many of the above simplifying assumptions may be relaxed in numerical simulations of the depth-averaged shallow fluid equations with shock-capturing algorithms, where complex

terrain and dam shapes, and frictional forces and possibly also entrainment/deposition, may be taken into account (see for example Gray and others, 2003). An insight into the simple situation analysed here is, nevertheless, useful in the interpretation of results from numerical simulations. The analytical expressions for dam height that are provided by the simplified analysis are also useful for developing initial ideas for dam geometry in more complex situations that can then be refined by numerical simulations.

3 Supercritical overflow versus a shock

A dry-snow avalanche will typically flow towards a dam in a supercritical state, that is with a Froude number Fr > 1 (or perhaps greater than some other limit larger than 1, depending on the rheology; the Froude number is defined in Eq. (4) below). The first determining factor for the design height of both catching and deflecting dams is that uninterrupted, *supercritical flow over the dam must be prevented*. If supercritical overflow is impossible, shallow fluid dynamics predict the formation of a shock upstream of the dam. This theoretical prediction has been confirmed for fluid and granular flow in several chute experiments, and may have been observed for natural snow avalanches. The second criterion for the design height of avalanche dams is that the *flow depth downstream of the shock, must be smaller than the dam height*. These two requirements in combination form the constitute of the design requirements that are proposed here and they are described in more detail in separate sections below.

The dynamics of the *formation* of a shock upstream of a dam is not well understood. In many, but not all, practical cases, the flow depth h_2 downstream of the shock is smaller than the dam height required to prevent supercritical overflow, assuming no loss of momentum in the impact with the dam. Therefore, if the formation of a shock could be guarantied by enough momentum dissipation, the dam could be built substantially lower than required for preventing supercritical overflow. However, there are indications from natural snow avalanches, which have overflowed or scaled high natural terrain obstacles, that avalanches can flow over dams higher than the flow depth downstream of a shock corresponding to likely values of the upstream velocity and flow depth. Therefore, it is proposed here to adopt a worst case scenario, firstly, supercritical overflow must be prevented during the initial interaction such that a shock may form, and then, overflow downstream of a shock must also be prevented.

4 The dynamics of flow against catching and deflecting dams

There is an obvious difference between the flow of avalanches against catching and deflecting dams that hides a fundamental dynamic similarity. This similarity partly shows up in the traditional expressions for the kinetic energy component of the vertical run-up above the snow cover, r, on dams in the design of catching and deflecting dams (Margreth, 2004)

$$r = h_1 + \frac{(u_1)^2}{2g\lambda} = h_1(1 + \frac{1}{2\lambda}\,\mathrm{Fr}^2\cos\psi)\ , \tag{1}$$

for catching dams, and

$$r = h_1 + \frac{(u_1\sin\varphi)^2}{2g\lambda} = h_1(1 + \frac{1}{2\lambda}\,(\mathrm{Fr}\sin\varphi)^2\cos\psi)\ , \tag{2}$$

for deflecting dams (the kinetic energy component is the second term on the right hand sides of the equations). The so-called λ-factor in these equations represents loss of kinetic energy in the interaction with the dam beyond the potential energy needed to scale the dam. These equations indicate that a deflecting dam is equivalent to a catching dam being hit by an avalanche with a velocity equal to the component of the velocity normal to the dam axis. The equations have an intuitively clear meaning for dams on horizontal terrain in terms of the kinetic and potential energy of a point-mass that moves over the dam. In that case, the vertical run-up, r, is equal to the run-up normal to the upstream terrain, h_r, in the notation of this report. However, for dams on sloping terrain, the equations do not have a similarly clear interpretation. This is evidenced by the fact that there are "potential streamlines" along the side of deflecting dams in sloping terrain that maintain the same altitude. If avalanches could flow along such streamlines, they would be able to overflow the dam without any loss of kinetic energy due to the scaling of the dam.

If friction is approximately balanced by downslope gravity as discussed above, the contact between the terrain and the bottom of the avalanche may be assumed to transmit only normal forces (within the framework of the depth-averaged description). Relative motion between the avalanche and the terrain, parallel with the terrain, has then no influence on the flow of the avalanche. This will be approximately true for regions with sharp gradients in the flow such as shocks, even when friction has some effect, if particles flow through the region in a very short time interval, compared with the time needed for frictional forces to have significant effect on the momentum of the flow. The conservation equations for mass and momentum for shallow fluid flow are equally valid in a uniformly moving coordinate system under these conditions. Let a ξ,η,ζ-coordinate system be defined such that the ξ-axis is aligned with the axis of a deflecting dam, the η-axis points in the direction normal to the dam axis in the upstream direction, the ζ-axis in the direction normal to the terrain as the z-axis, and the origin moves along the dam axis with speed $u_1\cos\varphi$ (see Figs. 2 and 3). It is easy to show that, for supercritical flow over the dam, the dynamics in the ξ,η,ζ-coordinate system are *exactly equivalent* to normal flow with uniform velocity $u_1\sin\varphi$ towards a catching dam. This fact may be used to express the criterion for supercritical overflow over a catching dam, in a form suitable for a deflecting dam.

The shock relations for a stationary, oblique hydraulic jump upstream of a deflecting dam may be similarly shown to be equivalent to a moving normal shock above a catching dam to

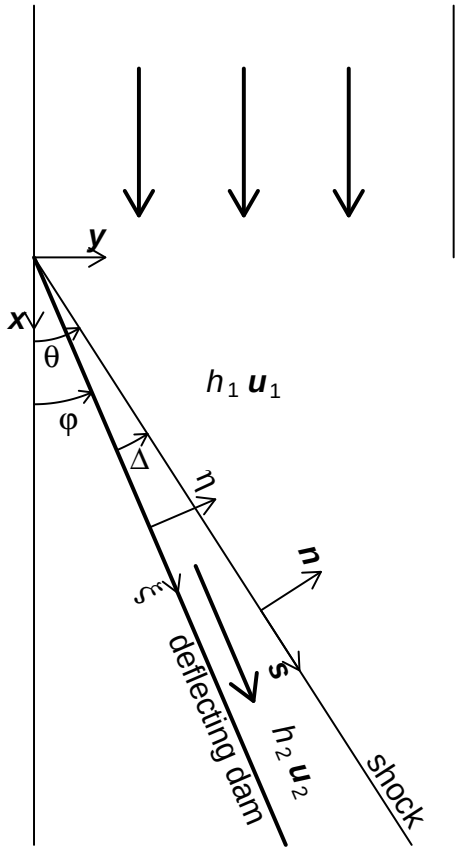

Figure 3: Schematic figure of an oblique shock above a deflecting dam showing the deflecting angle, φ, the shock angle, θ, their difference $\Delta = \theta - \varphi$, and the x,y-, ξ,η- and s,n-coordinate systems.

a very good approximation. This shows that avalanche flow against catching and deflecting dams are dynamically similar in a fundamental sense. This has the practical implication that theoretical derivations and results of laboratory experiments for catching dams may be used to improve design criteria for deflecting dams and vice versa.

5 Supercritical overflow: $H_{cr} + h_{cr}$

The height at which the avalanche changes from a supercritical flow state to a subcritical state when it hits a dam is here termed *critical dam height* and denoted by H_{cr} (Fig. 4). It can be derived from a conservation equation for the energy of the flow over the dam (see Hákonardóttir, 2004), which is valid if friction is balanced by gravity and as long as no shocks are formed,

$$H_{cr}/h_1 = \frac{1}{k} + \frac{1}{2}(k\,\mathrm{Fr}\sin\varphi)^2 - \frac{3}{2}(\mathrm{Fr}\sin\varphi)^{2/3}\ . \tag{3}$$

The critical dam height is the maximum height of a dam over which supercritical flow may be maintained. The Froude number is defined as

$$\mathrm{Fr} = \frac{u_1}{\sqrt{g\cos\psi\, h_1}}\ , \tag{4}$$

in terms of the velocity and flow depth of the oncoming flow. The coefficient k represents the loss of momentum normal to the dam axis in the impact and is discussed in Section 8 below. The momentum loss specified by k is only meaningful for dams that are higher than several times the upstream flow depth h_1. In the derivation of Equation (3), the momemtum loss is assumed to take place immediately as the flow crosses the foot of the dam.

The flow depth at height H_{cr}, above the snow cover at the base of the dam, here termed *critical flow depth* (Fig. 4), is given by

$$h_{cr}/h_1 = (\mathrm{Fr}\sin\varphi)^{2/3}\ . \tag{5}$$

The flow changes from a supercritical state to a subcritical state at the height H_{cr}, where the flow depth is h_{cr}, and the surface of the flow is at height $H_{cr} + h_{cr}$ above the snow cover. If the dam height above the snow cover is lower than H_{cr}, the main core of avalanche may overflow or "jump" over the dam in a supercritical state, and if the dam height is lower than $H_{cr} + h_{cr}$, the front of the avalanche may partly overflow the dam, while a shock is being formed. To prevent such overflow the dam height above the snow cover should be larger than $H_{cr} + h_{cr}$, which is given by

$$(H_{cr} + h_{cr})/h_1 = \frac{1}{k} + \frac{1}{2}(k\,\mathrm{Fr}\sin\varphi)^2 - \frac{1}{2}(\mathrm{Fr}\sin\varphi)^{2/3}\ , \tag{6}$$

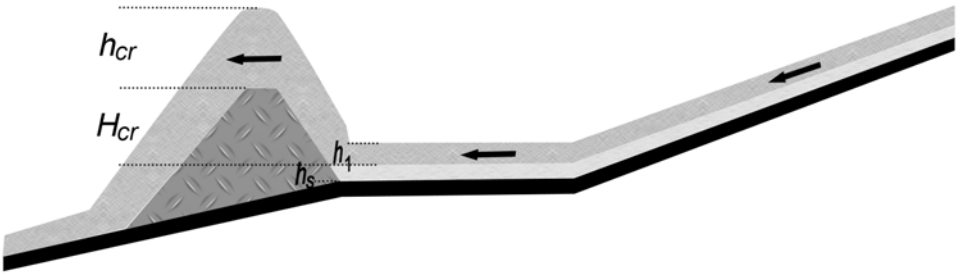

Figure 4: Schematic figure of supercritical overflow showing the critical dam height H_{cr} and the critical flow depth h_{cr}.

according to Equations (3) and (5).

The requirement expressed by Equation (6) may perhaps lead to some overdesign because a dam height of H_{cr} above the snow cover should be enough to form the shock. Overflow should then only occur temporarily and the bulk of the avalanche should be stopped or deflected. If some overflow can be tolerated, for example if the protected area is some distance away from the dam, it may be possible to require a dam height of only H_{cr} above the snow cover rather than $H_{cr}+h_{cr}$. It should, however, be borne in mind that overflow may occur in the initial impact of the avalanche front with the dam due to splashing for a dam height of $H_{cr}+h_{cr}$, so that even this dam height may not prevent some overflow of the dense core during the initial impact. In addition, some overflow will occur over most avalanche dams due to the saltation and powder components if the dams are hit by large avalanches. Whether H_{cr} or $H_{cr}+h_{cr}$ is the most appropriate dam height cannot be decided without more detailed understanding of the dynamics of the initial impact with the dam. Here, the more conservative choice is made and $H_{cr}+h_{cr}$ is adopted as a minimum dam height.

Equation (6) may be rewritten in dimensional form as

$$H_{cr}+h_{cr}=\frac{h_1}{k}+\frac{(u_1\sin\varphi)^2}{2g\cos\psi}k^2(1-k^{-2}(\mathrm{Fr}\sin\varphi)^{-4/3})\ , \tag{7}$$

which facilitates comparison with the traditional dam height expressions (1) and (2).

If a "Froude number" normal to the dam axis, $\mathrm{Fr}_\perp$, is defined as

$$\mathrm{Fr}_\perp=\mathrm{Fr}\sin\varphi=\frac{u_1\sin\varphi}{\sqrt{g\cos\psi h_1}}=\frac{|u_\eta|}{\sqrt{g\cos\psi h_1}}\ , \tag{8}$$

one may rewrite Equation (6) as

$$(H_{cr}+h_{cr})/h_1=\frac{1}{k}+\frac{1}{2}(k\,\mathrm{Fr}_\perp)^2-\frac{1}{2}(\mathrm{Fr}_\perp)^{2/3}\ , \tag{9}$$

which shows that the same fundamental expression, in terms of the component of the velocity normal to the dam axis, $u_\eta=u_1\sin\varphi$, may be used for both catching and deflecting dams. The equations are based on an assumption of energy conservation of the flow over the dam. The equations are thus only valid while the flow hitting the dam is supercritical and no shocks are formed, *i.e.* $(k^{3/2}\,\mathrm{Fr}_\perp)>1$.

Figure 5 shows the run-up for a deflecting dam according to Equation (6) as a function of the deflecting angle, φ, for several values of the upstream Froude number, Fr, and the run-up for a catching dam as a function of Froude number, Fr, (solid curves). The figure also shows run-up according to the traditional formula for the height of deflecting dams, Equation (2), with $\lambda=1$ (dashed curves). The lowering of the run-up derived from Equation (6), with respect to the corresponding run-up according to the traditional formula, is due to the thickening of the flow as it overflows the dam and the requirement that the overflow must be supercritical, which leads to a minimum flow velocity at the top of the dam. The resulting reduction in the required dam height is largest in a relative sense for low Froude numbers and low deflecting angles.

Equations (6) and (7) are similar in form to the traditional formulae (1) and (2), for the height of catching and deflecting dams above the snow cover, if the λ-factor is defined as

$$\lambda=\cos\psi\left(k^2(1-k^{-2}\mathrm{Fr}_\perp^{-4/3})+\frac{2}{k}(1-k)\,\mathrm{Fr}_\perp^{-2}\right)^{-1}\ . \tag{10}$$

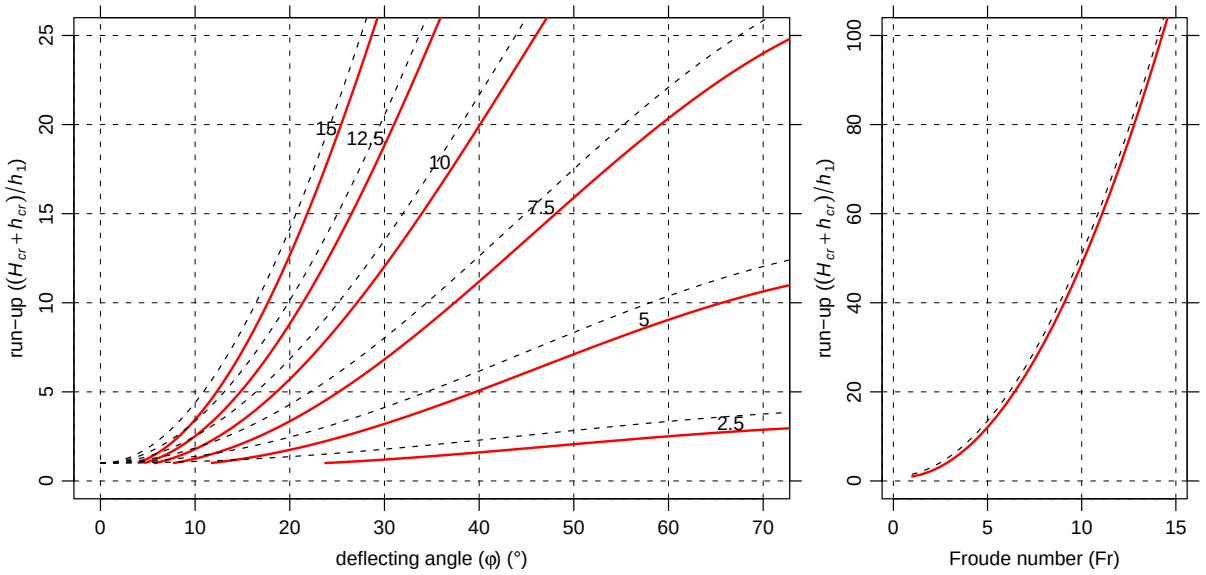

Figure 5: Supercritical run-up, $(H_{cr}+h_{cr})/h_1$, according to Equation (6), for a deflecting dam (left) as a function of deflecting angle and Froude number, and for a catching dam (right) as a function of Froude number, assuming no momentum loss in the impact ($k = 1$) (solid red curves). Dashed curves show run-up according to the traditional formulas for the height of avalanche dams (above the snow cover), Equations (1) and (2), for horizontal terrain ($\psi = 0$), also for no friction and no momentum loss in the impact ($\lambda = 1$). The curves for the deflecting dam are labelled with the Froude number Fr.

This expression predicts a λ-factor that changes from $\lambda \approx 1.1$ for $\mathrm{Fr}_\perp$ in the range 5–10, to $\lambda = 1.3$ for $\mathrm{Fr}_\perp = 3$, and $\lambda = 1.6$ for $\mathrm{Fr}_\perp = 2$ (assuming horizontal terrain ($\cos\psi = 1$) and no momentum loss in the impact ($k = 1$)). It thus requires somewhat lower dam heights compared with the traditional design expressions as $\mathrm{Fr}_\perp$ decreases. Deflecting dams with low deflecting angles sometimes correspond to quite low values of $\mathrm{Fr}_\perp$, even lower than 2. Then the dam height required by Equation (6) becomes quite low and the λ-factor may in this case be unexpectedly high. However, the requirement derived from flow depth downstream of the shock described in the next section will in this case be the determining factor for the design dam height.

Supercritical flow over dams was considered by Hungr and McClung (1987) and Chu and others (1995), who used a formula derived by Takahashi and Yoshida (1979) to propose an equation for the run-up of snow avalanches on dams, which they call the "leading-front model". Their equation predicts *higher* run-up on catching dams than the traditional dam height formula (1) in contrast to Equation (6). A detailed comparison of their derivation with a derivation based on energy conservation of supercritical flow without shocks shows that, although these authors *state* that supercritical flow is a condition for the validity of their model, they don't actually *use* this condition. In addition, they don't properly take the thickening of the flow as it flows up the dam side into account. Thus, the run-up predicted by the leading-front model can only be realised if the avalanche violates the assumptions that are stated in the derivation of the model. If the assumption of supercritical flow and the thickening of the flow are properly taken into account in the derivations of Hungr and McClung (1987) and Chu and others (1995), their analysis may be shown to be essentially equivalent with the dynamics underlying Equation (6).

6 Upstream shock: h_2

If the dam is high enough to prevent supercritical overflow, a propagating normal shock will form upstream of a catching dam and a semi-stationary, oblique shock may form upstream of a deflecting dam. The velocity and flow depth will change discontinuously across the shock according to the depth-averaged dynamics.

The conservation equations for mass and momentum for shallow, incompressible flow in 2D may be shown to lead to the following jump conditions across the shock (Whitham, 1999)

$$-[\![h]\!]\,c+[\![h\mathbf{u}]\!]\cdot\mathbf{n}=0 \tag{11}$$

and

$$-[\![h\mathbf{u}]\!]\,c+\left[\!\left[h\mathbf{uu}+\frac{1}{2}g\cos\psi h^2\mathsf{I}\right]\!\right]\cdot\mathbf{n}=0\,, \tag{12}$$

where the brackets are used to express the discontinuity in a quantity across the shock, for example $[\![h]\!]=h_2-h_1$, with the subscripts 1 and 2 denoting the upstream and downstream sides, respectively. $\mathbf{n}$ is a unit normal vector to the shock pointing in the direction of movement of the shock or in the upstream direction if the shock is stationary, $\mathbf{s}$ is a unit vector parallel to the shock (to be used below), and c is the propagation speed of the shock in the direction of $\mathbf{n}$ (see Fig. 3). $\mathbf{uu}$ denotes the tensor product of $\mathbf{u}$ with itself, which is sometimes denoted by $\mathbf{u}\otimes\mathbf{u}$, and I denotes the unit tensor. If the jump conditions are expressed in a reference frame that moves with the shock, so that the shock is stationary in this frame and thus $c=0$, they state that the component of the flux normal to the shock, is continuous across the stationary shock.

In a frame of reference moving with the shock, the jump conditions (11) and (12) simplify to

$$h_1u_{n_1}=h_2u_{n_2}\,, \tag{13}$$

$$h_1u_{n_1}u_{n_1}+\frac{1}{2}g\cos\psi h_1^2=h_2u_{n_2}u_{n_2}+\frac{1}{2}g\cos\psi h_2^2\,, \tag{14}$$

and

$$h_1u_{s_1}u_{n_1}=h_2u_{s_2}u_{n_2}\,, \tag{15}$$

where $u_n=\mathbf{u}\cdot\mathbf{n}$ and $u_s=\mathbf{u}\cdot\mathbf{s}$ are the components of the velocity normal and parallel to the shock, respectively, in the moving reference frame. These expressions are equally valid for shocks above catching and deflecting dams. Equations (13) and (14) may be shown to lead to the traditional equation for the height of a hydraulic jump (Chow, 1959)

$$(h_2/h_1)^2+(h_2/h_1)-2\mathrm{Fr}_n^2=0\,, \tag{16}$$

where $\mathrm{Fr}_n=|u_n|/\sqrt{g\cos\psi h_1}$ is the Froude number of the flow normal to the shock in the moving frame of reference where the shock is stationary. This equation has the well known solution

$$\frac{h_2}{h_1}=\frac{1}{2}(\sqrt{1+8\mathrm{Fr}_n^2}\;-1)\,. \tag{17}$$

The hydraulic jump solution cannot, however, be applied directly to shocks above catching and deflecting dams because the normal velocity, u_n, in the moving reference frame, which is used in the definition of Fr_n, depends on the speed of the shock, c, which is unknown and must

be determined as a part of the solution. Equation (15) is not needed much in the following analysis because the moving reference frame can, for both catching and deflecting dams, be chosen so that the component of the velocity parallel with the shock is identically equal to zero.

For a shock propagating upstream from a *catching dam* (with no overflow), the velocities in the reference frame moving with the shock, u_{n_1} and u_{n_2}, may be written in terms of the original velocities, u_1 and u_2, and the shock speed, c, as $u_{n_1} = u_1 + c$, $u_{n_2} = u_2 + c = c$. Using this, the shock condition (13) can be used to express the Froude number in the moving frame, Fr_n, as

$$\mathrm{Fr}_n^2 = (h_2/(h_2 - h_1))^2 \mathrm{Fr}^2 \, . \tag{18}$$

The hydraulic jump equation (16) can then be reformulated as

$$(h_2/h_1)^3 - (h_2/h_1)^2 - (1 + 2\mathrm{Fr}_\perp^2)(h_2/h_1) + 1 = 0 \, , \tag{19}$$

in terms of the original Froude number in the non-moving reference frame (Fig. 3). The Froude number is here denoted by $\mathrm{Fr}_\perp = \mathrm{Fr}\sin\varphi = \mathrm{Fr}\sin 90^\circ = \mathrm{Fr}$, rather than Fr, because this equation is also approximately valid for deflecting dams as will be shown below. Equation (19) assumes no change in the density of the flowing material as it comes to rest by the dam on the downstream side of the shock. A more general relationship, where a change in density may take place as the flow comes to rest above the dam, is given by Hákonardóttir (2004).

The shock relations for an oblique shock above a *deflecting dam* may be similarly derived by considering the equivalent, stationary, normal shock in a coordinate system, s, n, which is rotated by the shock angle, θ, with respect to the upstream flow direction (see Fig. 3), and moving with velocity $u_1 \cos\theta$ along the line defined by the shock (Chow, 1959; Whitham, 1999). This leads to the shock relations

$$\frac{u_2}{u_1} = \frac{\cos(\varphi + \Delta)}{\cos\Delta} \, , \quad \frac{h_2 u_2}{h_1 u_1} = \frac{\sin(\varphi + \Delta)}{\sin\Delta} \, , \quad \frac{h_2}{h_1} = \frac{\tan(\varphi + \Delta)}{\tan\Delta} \, , \tag{20}$$

where $\Delta = \theta - \varphi$ is the widening of the shock along the dam. The first relation expresses the requirement that the velocity component u_s in the direction parallel with the shock in the moving frame of reference must be identically equal to zero, because the dynamics in the moving frame are equivalent to a normal shock, where there is no flow in the direction parallel with the shock. This is equivalent to requiring the component of the velocity parallel to the shock in the non-moving reference frame to be continuous across the shock, which also follows from the jump condition (15) in combination with (13). The second relation is derived from the jump condition (13), which expresses the continuity of the mass flux across the shock and the last relation follows from the other two. Finally, the hydraulic jump condition (16), with $\mathrm{Fr}_n = \mathrm{Fr}\sin\theta = \mathrm{Fr}\sin(\varphi + \Delta)$, must be satisfied. Combining the last relation in (20) with the hydraulic jump solution (17), this leads to the following equation for Δ

$$\tan\Delta = \frac{2\tan(\varphi + \Delta)}{\sqrt{1 + 8\mathrm{Fr}^2 \sin^2(\varphi + \Delta)} - 1} = \frac{2\tan(\theta)}{\sqrt{1 + 8\mathrm{Fr}^2 \sin^2(\theta)} - 1} \, . \tag{21}$$

This equation is an implicit equation for Δ in terms of φ and Fr, and may, together with the last shock relation in (20), also be considered an implicit equation for h_2/h_1 in terms of φ for a given value of Fr. Figures showing θ, Δ and h_2/h_1 as functions of φ and Fr are given by

Hákonardóttir (2004) and Hákonardóttir and Hogg (2005). A derivation of the oblique shock relations (20) and a traditional somewhat more complex expression for θ in terms of φ and Fr, which is equivalent to (21), together with procedures to solve them graphically, are described by Chow (1959).

The close dynamic similarity of a propagating normal shock upstream of a catching dam and an oblique shock upstream of a deflecting dam may be analysed by considering the flow in the ξ,η-coordinate system, which is rotated by the deflecting angle, φ, with respect to the upstream flow direction (see Fig. 3). This is the same system as used in the previous section to analyse supercritical overflow, except that now the system is assumed to move parallel to the axis of the dam with speed equal to the velocity downstream of the shock, u_2. In this coordinate system, the speed of the oncoming flow towards the dam, normal to the dam axis, is given by $|u_\eta| = u_1 \sin\varphi$, and the material comes to an abrupt halt downstream of the shock, exactly as for a catching dam. The only difference is that the shock moves away from the dam at a small angle, Δ, from the direction normal to the axis of the dam, and the flow direction upstream of the shock also deviates from the direction normal to the dam by Δ. The angle Δ is in practice comparatively small for deflecting dams, and this difference enters the dynamic equations as second order terms in Δ such as $\sin^2\Delta$ and $(\cos\Delta - 1)$. Therefore, the dynamics of avalanche flow towards a deflecting dam are to a good approximation equivalent to the dynamics of normal flow towards a catching dam with speed $u_1 \sin\varphi$. This means that the flow depth h_2 downstream of the shock my be found from Equation (19) with $\mathrm{Fr}_\perp = \mathrm{Fr}\sin\varphi$. Equation (19) is a third degree polynomial equation in h_2/h_1, which may be solved with Cardano's method (see for example "`http://en.wikipedia.org/wiki/Cubic_equation`"). In this case, it has only one physically meaningful solution, which is given by

$$h_2/h_1 = (2\sqrt{(6\mathrm{Fr}_\perp^2 + 4)}\cos\delta + 1)/3 \,, \tag{22}$$

where δ is defined as

$$\delta = \frac{1}{3}\left(\frac{\pi}{2} - \tan^{-1}\left(\frac{9\mathrm{Fr}_\perp^2 - 8}{\mathrm{Fr}_\perp\sqrt{27(16 + 13\mathrm{Fr}_\perp^2 + 8\mathrm{Fr}_\perp^4)}}\right)\right) \,. \tag{23}$$

Having found the downstream shock flow depth from these equations, the angle Δ may be found to the same approximation from the last shock relation in (20) as

$$\Delta = \frac{\cos\varphi\sin\varphi}{\cos^2\varphi\,(h_2/h_1) - 1} \,, \tag{24}$$

from which the shock angle $\theta = \varphi + \Delta$ may also be found.

Figures 6 and 7 show the shock angle, θ, and the downstream flow depth, h_2, as functions of the deflecting angle, φ, for fixed values of the Froude number, Fr. The figures show both the exact oblique shock solution (20) and (21) (thin solid and dashed curves), and the explicit, approximate solution given by Equations (22) to (24) (thick curves) derived from the normal shock relation (19) with the Froude number $\mathrm{Fr}_\perp = \mathrm{Fr}\sin\varphi$. Figure 6 shows that two shock angles are possible for each pair of values of the deflecting angle and the Froude number. The shocks corresponding to the smaller and larger deflecting angle are called "weak" (thin solid curves) and "strong" (thin dashed curves) shocks, respectively (Chapman, 2000). The flow

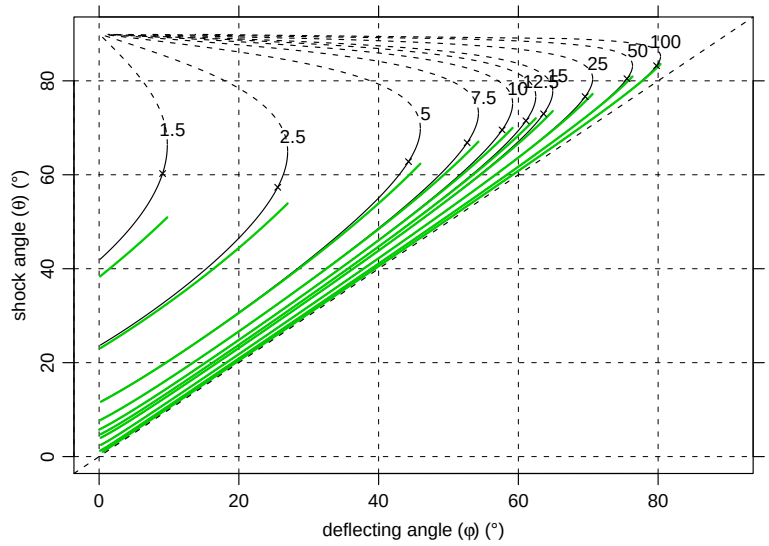

Figure 6: Shock angle θ as a function of deflecting angle φ for an oblique shock. Thin solid (weak shock) and dashed (strong shock) curves show the shock angle given by the oblique shock relations (20) and (21). Thick green curves show the results given by the approximate solution defined by Equations (22) to (24). The curves are labelled with the Froude number Fr and the ×-symbols show the values of the deflecting angle at which the flow downstream of the shock becomes critical.

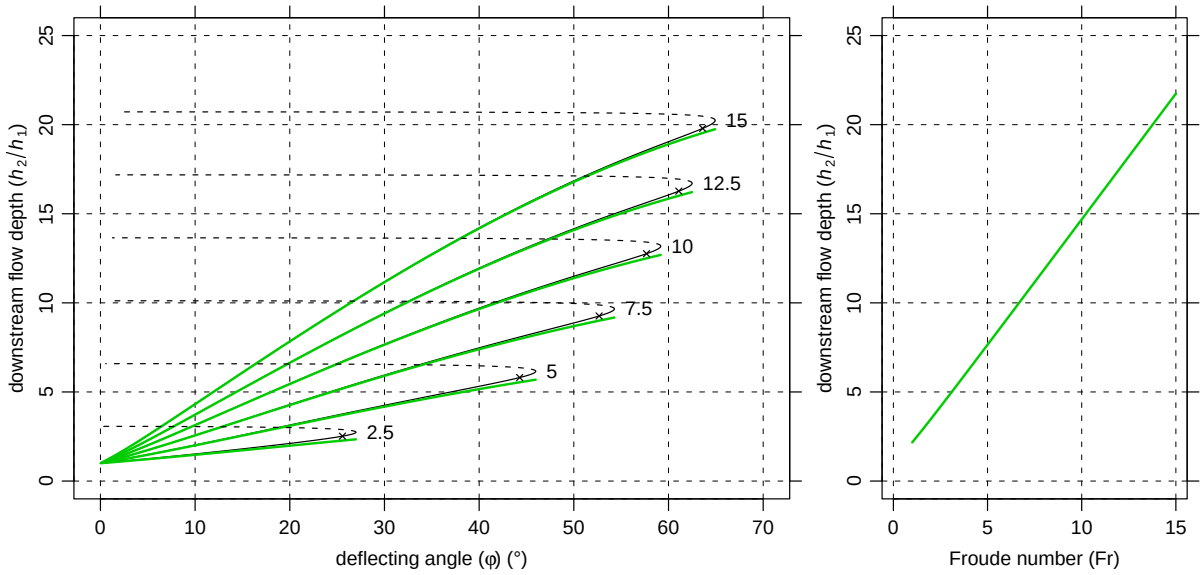

Figure 7: Flow depth downstream of an oblique shock for a deflecting dam (left) as a function of deflecting angle and Froude number, and for a catching dam (right) as a function of Froude number. Thin solid (weak shock) and dashed (strong shock) curves show the solutions given by the oblique shock relations (20) and (21). Thick green curves show the results given by the approximate solution defined by Equations (22) and (23). The curves for the deflecting dam are labelled with the Froude number Fr and the ×-symbols show the values of the deflecting angle at which the flow downstream of the shock becomes critical.

downstream of a strong shock is subcritical, but supercritical downstream of a weak shock, except in a narrow range close to the transition between the weak and strong shocks (see Figs.

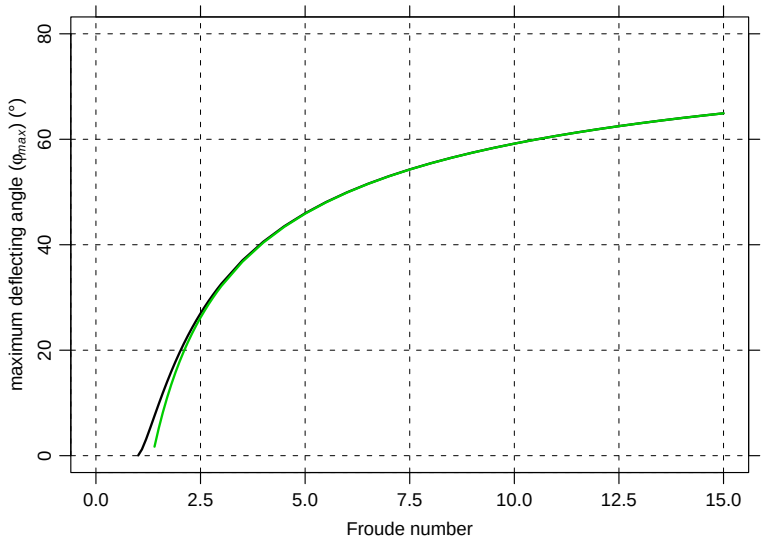

Figure 8: Maximum deflecting angle of an attached, stationary, oblique shock. The thick green curve shows the approximate solution defined by Equation (25).

6 and 7). The strong shock does typically not occur in real fluid or granular flow, but it has recently been observed experimentally in chute experiments with granular flow by adjusting the downstream flow conditions below the lower end of the dam (Xinjun Cui and Nico Gray, personal communication). The normal shock approximation given by (22) to (24) only gives the solution corresponding to the weak shock. Figures 6 and 7 show that the normal shock dynamics provide a good approximation to the exact oblique shock solution for $\mathrm{Fr} \geq 2.5$ and deflecting angles, φ, somewhat below the boundary between the weak and strong shocks (*cf.* Figs. 6 and 7). Thus, the normal shock approximation more or less covers the range in Fr and φ that is relevant for deflecting dams.

For each value of the Froude number, Fr, an attached, stationary, oblique shock is not dynamically possible for deflecting angles, φ, larger than a maximum, $\varphi_{\max}$, which represents the boundary between the weak and strong shocks in Figures 6 and 7. The deflecting angle corresponding to this maximum may be approximately evaluated as (Hákonardóttir and Hogg, 2005)

$$\varphi_{\max} = \frac{\pi}{2} - \frac{2^{3/4}}{\mathrm{Fr}^{1/2}} - \frac{2^{1/4}}{6\,\mathrm{Fr}^{3/2}} + O\left(\frac{1}{\mathrm{Fr}^{5/2}}\right) . \tag{25}$$

The maximum deflecting angle derived from Equation (21) (black curve) and approximately by Equation (25) (green curve) is shown as a function of the Froude number Fr in Figure 8. Chute experiments with granular materials indicate that an attached, stationary shock may perhaps not be maintained for deflecting angles close to the theoretical maximum, $\varphi_{\max}$. Therefore, it is recommended here that dam deflecting angles should be at least 10° lower than $\varphi_{\max}$. An avalanche hitting a dam with a deflecting angle φ that does not satisfy this requirement may not remain attached and start to propagate upstream to form a detached, semi-stationary shock (Chapman, 2000). The detached shock will form a larger angle with respect to the oncoming flow than an attached shock and, therefore, the jump in flow depth across the shock will also be larger. It is recommended here that the downstream shock depth for a dam that does not satisfy the above requirement for an attached, semi-stationary, oblique shock be computed as for a catching dam with $\varphi = 90^\circ$. The criterion based on supercritical

Figure 9: A granular avalanche with Fr ≈ 13.5 hitting a deflecting dam with $\phi = 20^\circ$ in a laboratory chute at the Hydraulics and Environmental Engineering Dept. of the University of Pavia.

overflow is, however, computed with the original value of φ as before (see Section 5).

The similarity of the normal and oblique shock dynamics, which is evident from Figures 6 and 7, is also manifested in results of laboratory experiments in chutes of various sizes. The interaction of granular avalanches and water flows with deflecting dams near the upstream end of the dam is characterised by an adjustment region (see Hákonardóttir and Hogg, 2005), within which the normal distance to the dam is less than the width of the transition region between the two flow states farther downstream. Within this region, the continuation of the surface of the oncoming flow may be clearly distinguished as the flow overturns and falls back on itself (see Fig. 9), and the run-up on the dam can be higher than farther downstream, particularly for high Froude numbers and large deflecting angles. If this adjustment region is viewed from a coordinate system moving downstream parallel with the dam as described above, then this region is, apart from splashing in the impact, dynamically equivalent to the initial impact of an avalanche with a catching dam during the formation of the normal shock, which is often characterised by similar backwards rotation in the flow.

As for the dam height expression derived from the analysis of supercritical overflow in the previous section, flow depth derived from the shock relations (20) and (21), or from Equations (22) and (23), may be compared with the traditional dam design formulae (1) and (2). By solving Equations (22) and (23) for λ and substituting r by h_2 one obtains the following expression for the λ-factor

$$\lambda = \frac{h_1 \mathrm{Fr}_\perp^2 \cos\psi}{2(h_2 - h_1)} \,. \tag{26}$$

This equation may be used to compare the results of the traditional formulae with the results derived from shock dynamics.

Shallow fluid shock theory has not been applied to the design of avalanche dams until recently. This theory has, on the other hand, been applied in hydraulics for many decades and it is the basis of the design of numerous hydraulic structures of different types and scales (see for example Chow, 1959; Hager, 1992). The theory has in this context been thoroughly verified for fluid flow. Somewhat unexpectedly, recent chute experiments indicate that the shallow

fluid shock theory provides an even better approximation to granular flows than to fluid flows, for which the theory was originally developed (see Hákonardóttir and Hogg, 2005). This arises because of rapid frictional dissipation in the interaction between grains that can occur in shocks in granular media, which appears to be a more efficient dissipation mechanism than fluid friction. Transition zones with deviations from the theoretically predicted discontinuities in velocity and flow depth are, therefore, narrower in granular flows than in fluid flows. There are of course many aspects of snow avalanche dynamics that are not adequately described by shallow fluid dynamics applied to the dense core as mentioned in the Introduction and Background sections. Nevertheless, it is clear from the theoretical and experimental studies that have been summarised here that dam height requirements derived from shallow fluid dynamics should be viewed as minimum requirements for avalanche dams.

7 Comparison with traditional design formulae

The λ-factors defined in Equations (10) and (26) are shown in Figure 10 in order to compare the design criteria based on supercritical overflow (red curves, decreasing λ-factor from left to right) and shock dynamics (green curves, increasing λ-factor from left to right) with the traditional design formulae for avalanche dams (1) and (2). Solid curves indicate the combined design criteria corresponding to the higher of the two dam height requirements in each case. As before, horizontal terrain ($\psi = 0$) and no momentum loss in the impact with the dam for supercritical overflow ($k = 1$) are assumed. Momentum loss in the impact will be discussed in Section 8.

A λ-factor equal to 1 corresponds to dam height identical to the traditional formulae, $\lambda < 1$ means that the new criteria require higher dams than the traditional ones, and $\lambda > 1$ means that the new criteria lead to lower dams than before. Figure 10 (right) shows that supercritical run-up is the determining factor for the dam height for Froude numbers above a certain value of Fr, which depends on the deflecting angle, at which there is a kink in the thick curves (at the point where the color of the thick curve changes from green to red). Flow depth downstream of the shock determines the dam height for lower Froude numbers. Compared with the traditional design formulae, supercritical overflow becomes less important for low Froude numbers and low deflecting angles, whereas the reverse it true for overflow due to flow depth downstream of the shock by the dam. When the combined criteria (thick curves) are considered, the main difference with respect to the traditional formulae is that considerably higher dams are required for low deflecting angles at relatively low Froude numbers. As an example, deflecting dams with $\varphi = 20°$ corresponding to $\mathrm{Fr} = 5$, or $\varphi = 10°$ and $\mathrm{Fr} = 10$,

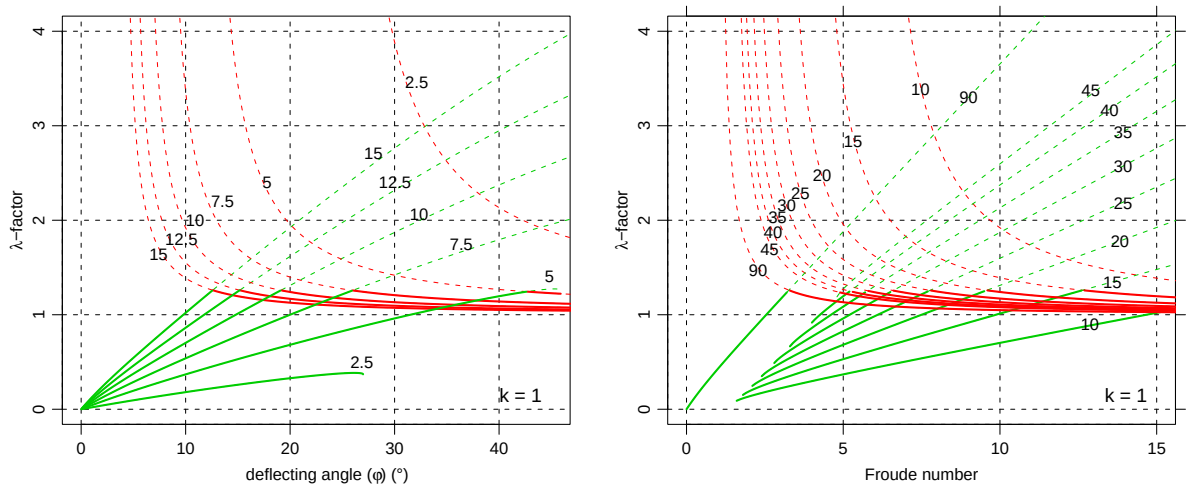

Figure 10: The λ-factor as a function of φ (left) and Fr (right) corresponding to both supercritical overflow (red curves) and shock dynamics (green curves). The curves are drawn for horizontal terrain ($\psi = 0$) and assuming no momentum loss in the impact ($k = 1$). The part of each pair of curves for the same Froude number (left) or deflecting angle (right) corresponding to the lower λ-factor (larger dam height) is drawn as a solid thick curve. The curves in the figure to the left are labelled with the Froude number and with the deflecting angle in the figure to the right. The curves for deflecting dams derived from oblique shock dynamics (green) only show λ-factors corresponding to $\varphi < \varphi_{\max}$, where an attached, stationary, oblique shock is possible.

need to be built approximately one third higher according to the new criteria compared with the traditional formulae. This is, however, not as significant a change as it seems at first sight, because the run-up component of the dam height is much smaller for these combinations of φ and Fr than for larger deflecting angles. The difference between the new and old criteria may, for example, lead to an increase in run-up, h_r, above the snow cover from 6–8 m to 9–10 m.

8 Loss of momentum in the impact with a dam: k

The discussion has so far assumed no loss of momentum (or equivalently kinetic energy) in the impact with the dam ($k = 1$ in Equations (6) and (7)). This is a worst case scenario and leads to the highest dams. It is a pessimistic design assumption where the flow of granular material is forced to change direction abruptly. Chute experiments with granular materials, including a few experiments with snow (Hákonardóttir, 2004, section 6.4; Hákonardóttir and others, 2003), indicate that a substantial reduction in flow velocity occurs in the impact with steep catching dams that are overflowed by avalanches. This reduction is beyond the reduction in kinetic energy corresponding to the potential energy needed to overflow or scale the dam. These experiments indicate that approximately 50%, or even more (see Hákonardóttir and others, 2003), of the kinetic energy of a granular avalanche is lost in an impact with dams that are positioned normal to the bottom of the experimental chute and have heights greater than 2 to 3 times the flow depth. Furthermore, dams that have steep upstream faces with $\alpha \geq 60^\circ$ seem to be as, or almost as, efficient energy dissipators as dams with upstream faces normal to the terrain, at least for the granular material that was used in these experiments (glass beads). Dams with $\alpha = 30^\circ$ were, on the other hand, found to be less efficient. These results provide an estimate of the velocity reduction that takes place as a consequence of the abrupt change in flow direction at the upstream foot of a dam. As such, they can be used to estimate the relative reduction in velocity between the oncoming flow and the avalanche as it flows up the dam side after leaving the impact region at the bottom of the dam. There is, however, a considerable uncertainty applying the results to natural-scale snow avalanche defence dams. The chute experiments indicate a somewhat *greater* reduction in velocity than can easily be reconciled with some field observations of run-up of snow avalanches on dams and obstacles in the natural terrain (see discussion at the end of the section). They are, however, the only available direct evidence on the basis of which values of k can be estimated.

It is important to note that the choice of k only affects the run-up requirement corresponding to supercritical overflow (Eq. (6)). The dam height requirement arising from the flow depth downstream of the shock is not affected by the choice of k. In fact, chute experiments have shown that the flow depth downstream of the shock for deflecting dams with sloping sides ($\alpha < 90^\circ$) is the same as for steep dams (see Hákonardóttir, 2004). Therefore, the change in the required dam height by adopting a value of $k < 1$ is most important for catching dams, but the design height of deflecting dams is much less affected.

The λ-factor in the traditional design formula for catching dams (1) has often been chosen approximately 1.5 for catching dams built from loose materials with a slope of the upstream side close to 1:1.5 ($\alpha = 34^\circ$ on horizontal terrain), and approximately 2 for steep dams with a reinforced upstream side with a slope greater than 2:1 ($\alpha = 63^\circ$ on horizontal terrain). For deflecting dams, it is often assumed that $\lambda = 1$, that is no loss of momentum in the impact. These λ-values for catching dams are in rough agreement with the results of the chute experiments described above. The λ-value 1.5 corresponds to $k \approx 0.85$, for catching dams from loose materials with a slope of 1:1.5, and $\lambda = 2$ corresponds to $k \approx 0.75$, for steep catching dams with a slope of 2:1 or greater, in the dam height expression (6). These values take into account the effect of the thickening of the flow during run-up, which leads to $\lambda > 1$ according the supercritical overflow criterion, even when $k = 1$ (see Fig. 10).

Momentum loss in the impact is not well understood dynamically, so not much guidance for the determination of k can be obtained from theory. The approximate dynamic equivalence

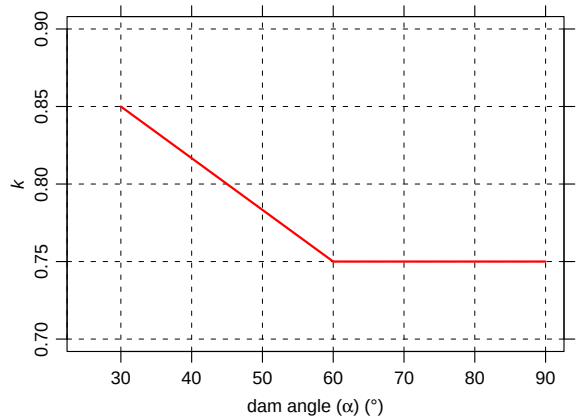

Figure 11: Momentum loss factor k as a function of dam angle α according to Equation (27). k is not defined for $\alpha < 30^\circ$.

of catching and deflecting dams, which was discussed in the previous section, indicates, however, that the momentum loss should be applied to both catching and deflecting dams. On the basis of the chute experiments described above and based on observations of run-up of natural snow avalanches (see below), it is proposed here that, for dry-snow avalanches, $k = 0.75$ is used for dams with $\alpha > 60^\circ$, and $k = 0.85$ for dams with $\alpha = 30^\circ$, with a linear interpolation for slopes between these points. This variation of k is expressed with the following equation

$$k = 0.75 \text{ for } \alpha > 60^\circ \ , \quad k = 0.75 + 0.1(60^\circ - \alpha)/30^\circ \quad \text{for} \quad 30^\circ \leq \alpha \leq 60^\circ \ , \qquad (27)$$

and shown graphically in Figure 11. Dams with side slopes lower than $\alpha = 30^\circ$ should, in general, not be built, so that it is not necessary to choose k for lower values of α.

The above recommended values of k are intended for dry-snow avalanches. Similar, explicit, recommended values of k for wet-snow avalanches are not given here and need to be decided on a case-by-case basis. There may be less energy dissipation at the foot of the dam for wet-snow avalanches due to the greater cohesion of wet snow compared with dry snow and, therefore, a k value equal to 1 would perhaps be an appropriate conservative choice. Since wet-snow avalanches tend to move slower than dry-snow avalanches, avalanche speed, and thus the choice of k, is not a determining factor for the dam height in many cases. Flow depth of wet-snow avalanches downstream of a shock formed along a damside (to the extent that such a shock is formed) may be expected to be governed by the same dynamics as for dry-snow avalanches so the requirements arising from shock dynamics should be equally valid for wet- and dry-snow avalanches and should be considered to provide a lower bound on the dam height. Explicit dam height recommendations for wet-snow avalanches are not developed here from dynamic principles but qualitative recommendations for dams intended as protection agains wet-snow avalanches are given in the SATSIE handbook.

Figure 12 shows λ-factors derived for momentum loss in the impact with the dam corresponding to the chosen values of $k = 0.85$ (dams of loose materials) and $k = 0.75$ (steep dams). Comparison with Figure 10 shows that the curves derived from supercritical overflow have been shifted upwards so that the run-up height is now determined by the flow depth downstream of the shock for a larger range of Froude numbers. The curves derived from shock dynamics are, however, not changed from Figure 10. In the most relevant range of Froude numbers for snow avalanches, $5 \leq \text{Fr} \leq 10$, the height of deflecting dams built from

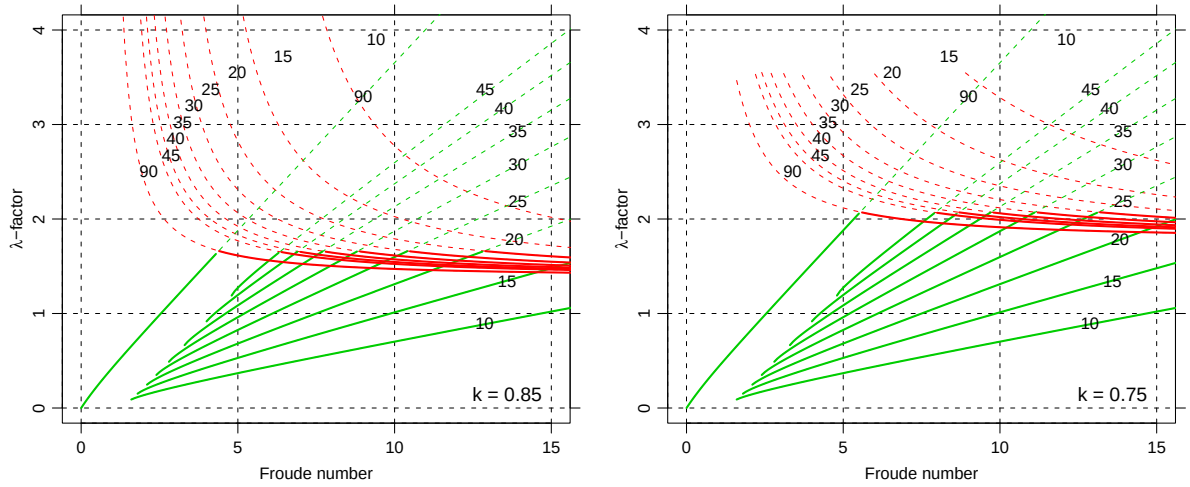

Figure 12: The λ-factor as a function of Fr for given values of φ, assuming momentum loss in the impact with the dam with $k = 0.85$ (left, corresponding to dams built from loose materials) and $k = 0.75$ (right, corresponding to steep dams). The figures show curves derived from both supercritical overflow (red curves) and shock dynamics (green curves). See the caption of Figure 10 for further explanations.

loose materials ($k = 0.85$) is primarily determined by shock dynamics for deflecting angles $\varphi < 25^\circ$. For deflecting angles in the range $25 \leq \varphi \leq 35$–40°, both supercritical overflow and shock dynamics are important, depending on the Froude number. Higher deflecting angles than 35–40° are most often not compatible with the requirement that φ should be at least 10° below φ_{max}.

Figure 13 shows a comparison of the run-up expressions derived from supercritical overflow (with k according to Eq. (27) for paths with an abrupt change in slope at the foot of the obstacle) and the flow depth downstream of a shock with field observations of run-up of 22 natural snow avalanches in Norway, Iceland and France on dams and terrain obstacles. These field observations are further described in Section 14 and in the references quoted in the figure caption. Many of the obstacles are situated on rather steep terrain where there is a significant difference between run-up normal to the upstream terrain (here denoted by h_r) and vertical run-up (here denoted by r and traditionally measured in a vertical cross section normal to the dam axis in the map plane). The figure shows vertical run-up since this is the quantity reported in reports about the avalanches. The theoretically predicted run-up normal to the terrain has been transformed to the corresponding vertical run-up (see expressions in the section about these avalanches below). The flow depth, h_1, and velocity, u_1, of the oncoming flow are unknown for all the avalanches and must be considered quite uncertain. The velocity was estimated by modelling and the flow depth subjectively, with some assistance from modelling for some avalanches. In order to highlight the uncertainty due to these estimates, the model results are depicted as ranges corresponding to subjectively chosen ranges in h_1 (most often 1–3 m) and u_1 (±15%) rather than as single values. The figure clearly shows that the ranges in computed run-up corresponding to "moderate" variations in h_1 and u_1 are quite large.

The run-up of several of the avalanches is higher than the theoretically predicted run-up ranges, but many of them fall within the predicted ranges as further discussed in the section about the run-up data set. Momentum loss in the impact is only assumed for paths with an abrupt change in slope at the foot of the obstacle (marked with "(*)" in legend of Figure

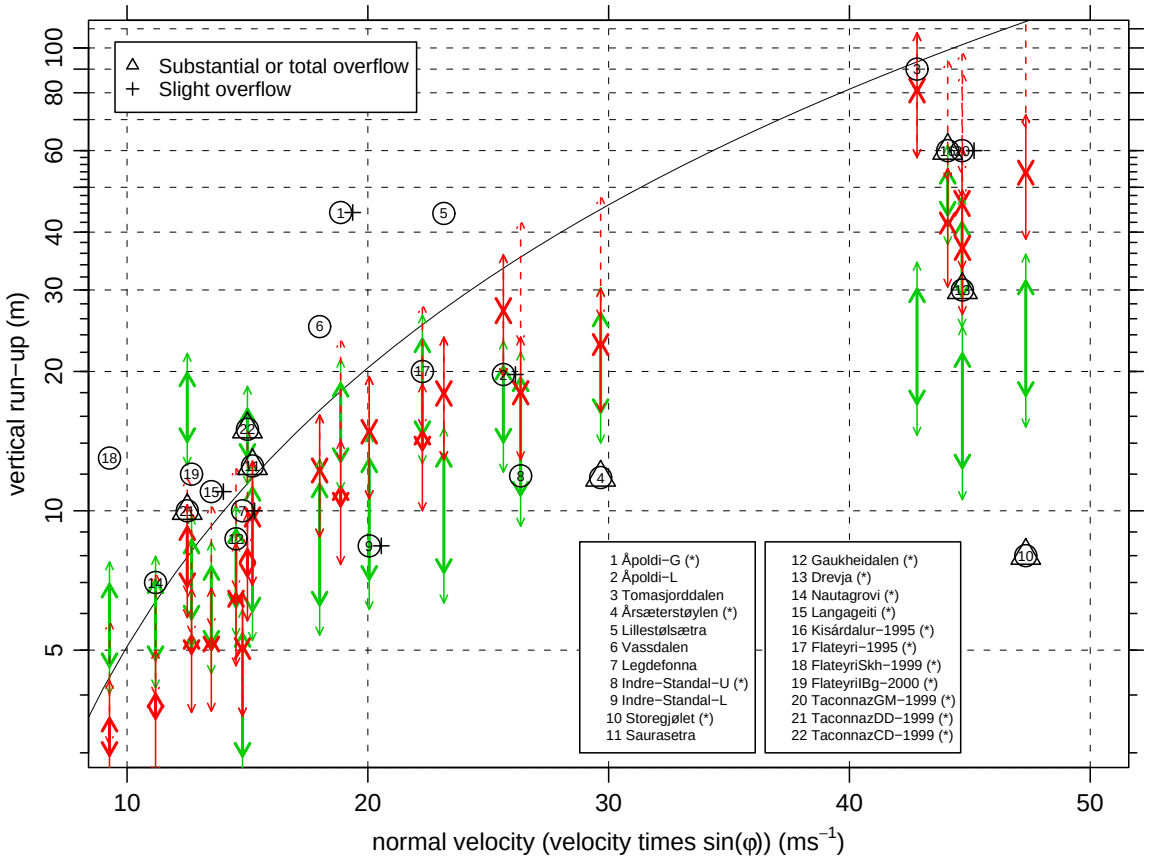

Figure 13: Run-up of natural snow avalanches in Norway (Harbitz and Domaas, 1997; Domaas and Harbitz, 1998; Harbitz, Domaas and Engen, 2001; Harbitz and Domaas, in prep.), Iceland (Jóhannesson, 2001) and France (Mohamed Naaim and Francois Rapin, personal communication 2006) on dams and terrain features compared with results of the run-up expressions derived from supercritical overflow (Eq. (6) with k determined from Eq. (27) for the avalanches where momentum loss in the impact is assumed) and the flow depth downstream of a shock (Eqs. (22) and (23)). Momentum loss in the impact with the obstacle is only assumed for paths with an abrupt change in slope at the foot of the obstacle (marked with "(*)" in figure legend). Symbols with numbers denote observed vertical run-up. Overflow, where a substantial part or the entire avalanche went past the obstacle, is denoted with $\triangle$, and slight overflow is denoted with $\oplus$. Double arrows denote (somewhat arbitrary) ranges in the estimates for the flow depth, h_1 (typically 1–3 m), and velocity, u_1 ($\pm 15\%$), of the oncoming avalanche. Thick arrows correspond to the range in h_1 only, using the central estimate for u_1 from the above references. Thin arrows correspond to ranges in both h_1 and u_1. For the avalanches where momentum loss is assumed in the impact, the run-up range corresponding to no momentum loss is shown with dashed thin arrows. Run-up ranges derived from supercritical overflow are shown with red arrows and ranges derived from flow depth downstream of a shock with green arrows. Run-up ranges corresponding to ranges in u_1 are in all cases drawn at the location corresponding to the central estimate for u_1, so that the symbol, indicating the observed run-up, and both arrows for each avalanche are drawn at the same location on the x-axis in the figure (same value of the normal velocity $u_\eta = u_1 \sin\varphi$).

13). This is the case for all the man-made dams (six avalanches in total), and for six of the Norwegian avalanches hitting natural obstacles, the Kisárdalur and Flateyri avalanches from Iceland in 1995, and the Taconnaz avalanche hitting the glacier moraine (see the section about

the data set below for further explanations). Two of those avalanches (no. 4 and 10) overflowed obstacles that are considerably lower than the theoretically predicted run-up. The high run-up on the deflecting dams at Flateyri in 1999 and 2000 (no. 18 and 19) may perhaps be explained by the run-up marks on loose snow on the dam sides being caused by the saltation layer of the avalanche rather than by the dense core. Three of the remaining eleven avalanches (no. 13, 21 and 22) overflowed obstacles with height within or lower than the theoretically predicted ranges, five avalanches (no. 8, 12, 14, 17, 20) produced run-up marks within the ranges or close to them, one avalanche (no. 15, Langageiti) slightly overflowed an 11 m high dam for which the upper limit of the predicted ranges is approximately 8.5 m, one avalanche (no. 1, Åpoldi-G) produced *much higher* run-up marks than theoretically predicted, even when no momentum loss is assumed, and one avalanche (no. 16, Kisárdalur) *completely overflowed an obstacle*, which is *higher than the predicted run-up range*, when momentum loss in the impact is assumed.

The run-up data can, thus, only be partially reconciled with the theoretically predicted run-up ranges. Dashed arrows in Figure 13 show the run-up range corresponding to no momentum loss in the impact for the avalanches hitting abrupt obstacles. The difference between the dashed and solid ranges clearly shows the large effect of the assumed momentum loss. Similarly, relatively small modifications in the assumed velocity of the avalanches can results in substantial changes in the predicted run-up ranges. Uncertainty in the flow depth, on the other hand, has little effect on the predicted run-up, except for the Kisárdalur and Taconnaz avalanches, which are estimated and/or modelled to have been unusually thick. The Kisárdalur avalanche (no. 16) is in the lower part of the dashed range but the Åpoldi-G avalanche (no. 1) is far above the dashed range and is very difficult to reconcile with the theoretical predictions. According to NGI reports, the run-up marks of the Åpoldi-G avalanche are likely to have been produced by the powder part of the avalanche so is not certain that the dense core reached this high.

Except for the Åpoldi-G avalanche, the assumed momentum loss, leads to run-up ranges that are in rough agreement with this limited data set, with some avalanches within or at the lower end of the ranges, and some above, whereas no momentum loss leads to rather high ranges for the avalanches that hit abrupt obstacles. The Taconnaz avalanche hitting the glacier moraine in 1999 is in the upper part of the range corresponding to supercritical overflow, when momentum loss is assumed. Since this is a very large avalanche and the deflecting angle is rather large ($\approx 40^\circ$), this point on Figure 13 indicates that the theory leads to reasonable run-up predictions for very large events with large normal velocities, and thus is not limited to laboratory-scale granular flows or small snow avalanches. The avalanche at Flateyri in 1995 is also quite large and hits a steep gully wall at a rather large deflecting angle ($\approx 30^\circ$) with a run-up that falls within the predicted range. On the other hand, the rather wide spread of the data points compared with the assumed uncertainty of the theoretical predictions clearly indicates an incomplete understanding of the dynamics of the impact process. The Åpoldi-G and the Kisárdalur avalanches, in particular, represent worrisome data points. Another worrisome observation is provided by a medium-sized avalanche in Seyðisfjörður, eastern Iceland, in April 2006, which overflowed a 20 m high catching dam, with a steep uppermost 10 m of the upstream side, leaving little stopped snow on the upstream side of the dam. This avalanche has not yet been modelled and it is, therefore, not included in the data set shown in Figure 13. Two other avalanches with the largest run-up in excess of the theoretically predicted run-up ranges (no. 5 and 6) did not hit abrupt obstacles. They are further discussed in Section 14.

9 Combined criteria: supercritical overflow and shock flow depth: $\max(H_{cr}+h_{cr}, h_2)$

Figures 5 and 7 represent the two dam height requirements proposed in Sections 5 and 6. The figures for deflecting dams have the same scales and can therefore easily be compared. Since both requirements must be satisfied, the larger dam height corresponding to a given pair of a Froude number and a deflecting angle must be chosen for each dam under consideration. For high Froude numbers and large deflecting angles, the criterion derived from supercritical overflow leads to the higher dam, but for low Froude numbers and small deflecting angles, the shock criterion leads to the higher dam.

The right panels of Figures 5 and 7 that show run-up height for catching dams have different scales for the y-axis. Figure 14 shows both the supercritical run-up, $(H_{cr}+h_{cr})/h_1$, according to Equation (6), and the flow depth downstream of a normal shock, h_2/h_1, according to Equations (22) and (23), for a catching dam, both as functions of the Froude number, Fr. The figure shows that supercritical run-up is the determining factor for the design height of catching dams for Froude numbers above approximately 3, but flow depth downstream of the shock determines the dam height for lower Froude numbers.

The combined requirements derived from supercritical overflow and flow depth downstream of a shock are expressed graphically in Figure 15 for both dams from loose materials ($k = 0.85$, left) and steep dams ($k = 0.75$, right). The design dam height above the snow cover, $h_r = H - h_s$, corresponding to given values of h_1 and $|u_\eta| = u_1 \sin\varphi$, may be read directly from the higher one of two curves in each figure that represent supercritical overflow (red curves) and flow depth downstream of a shock (green curves), respectively. The same curves may be used for both catching and deflecting dams because of the use of the normal shock approximations (22) and (23), according to which run-up on a deflecting dam depends only on the

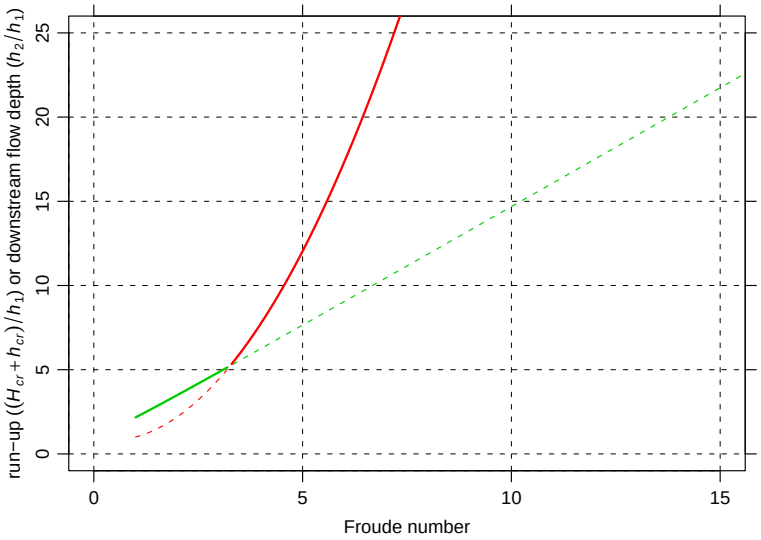

Figure 14: Supercritical run-up, $(H_{cr}+h_{cr})/h_1$, according to Equation (6) (red curve), and flow depth downstream of a normal shock, h_2/h_1, according to Equations (22) and (23) (green curve), as functions of Froude number, Fr, for a catching dam. The curve for supercritical run-up is drawn assuming no momentum loss in the impact ($k = 1$). The part of each curve corresponding to larger dam height is drawn as a solid thick curve.

component of the velocity normal to the dam axis in the same manner as for a catching dam.

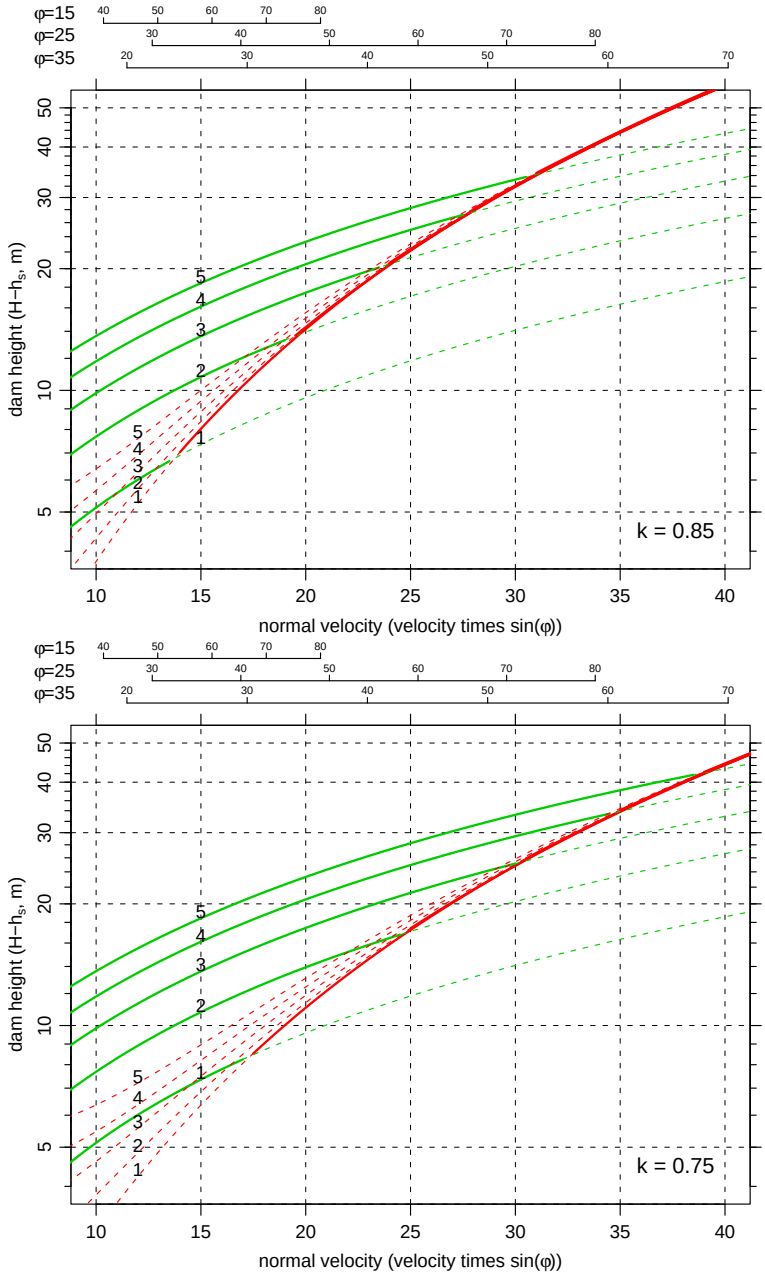

Figure 15: Design dam height (normal to the terrain) above the snow cover $H - h_s$ as a function of the component of the velocity normal to the dam axis, $|u_\eta| = u_1 \sin\varphi$, for several different values for the depth of the oncoming flow h_1. Momentum loss in the impact with the dam is assumed with $k = 0.85$ (upper panel, corresponding to dams built from loose materials) and $k = 0.75$ (lower panel, corresponding to steep dams). The figures show curves derived from both supercritical overflow (red curves) and shock dynamics (green curves) labelled with the flow depth h_1. The design dam height should be picked from the higher of the two curves corresponding to the estimated design flow depth. The part of each family of curves corresponding to the higher dam is drawn with solid, thick curves. The labelled axes at the top of the figures show velocity corresponding to the deflecting angles $\varphi = 15$, 25 and 35°. Note the logarithmic scale on the y-axis.

Labelled axes at the top of the figure show the upstream velocity u_1 corresponding to three deflecting angles for convenience.

The dependence of the dam height on the upstream flow depth h_1 according to the dam height criteria shown in Figure 15 is somewhat different from the traditional criteria (1) and (2). According to the traditional criteria, the upstream flow depth affects the dam height simply as an additional term equal to h_1. The flow depth enters the new criteria in a different way, and at first sight it appears to be a multiplicative quantity in both the criterion that arises from supercritical overflow and flow depth downstream of the shock (Eqs. (7) and (22)). Figure 15 shows, however, that the expression arising from supercritical overflow predicts a weak dependency of the dam height on flow depth, particularly for high velocities, as was also seen in Figure 13. This is due to a partial cancellation of terms in the dam height expression (7). The dam height derived from flow depth downstream of the shock depends, however, linearly on h_1, for a given Froude number, but approximately linearly on the square root of h_1 for a given upstream velocity u_1.

10 Terrain slope towards the dam: $\Delta H_{\psi_\perp}$

It is implicitly assumed in the preceding analysis that the downslope component of gravity is approximately balanced by friction. Thus, all formulas describing supercritical overflow and formation of a shock by the dam have been derived without regard to the downslope component of gravity or to friction. For supercritical overflow, one may assume that for each part of the avalanche, the impact does not last long enough for frictional forces to reduce the momentum of the flow significantly. For a normal shock upstream of a catching dam where the terrain slope is smaller than the internal friction angle of avalanching snow, ϕ, one may assume that the propagation of the shock away from the dam will not be much affected by the slope of the terrain because the snow downstream of the shock is stopped. For flow downstream of an oblique shock by a deflecting dam on sloping terrain, one may, however, expect the assumption of an approximate balance of downslope gravity by friction to fail. This arises because the direction of the flow downstream of the shock is parallel to the dam and friction arising in this flow can, therefore, not balance the component of gravity normal to the dam axis. Furthermore, the material does not stop by the dam as for a catching dam so that there should in general be sufficient agitation in the flow that the material may be expected to flow towards the dam and form an approximately horizontal profile from the shock towards the dam in the direction normal to the dam axis (Fig. 16).

The shock height will in this case still satisfy the hydraulic jump equation (16) but the Froude number in the moving frame of reference, Fr_n, must be evaluated taking into account the flow of material across the shock towards the dam that is needed to form the horizontal profile. The flow will not fully achieve a horizontal profile, but this limiting case is analysed here since it is the worst case scenario with respect to the required dam height. Also, the shock front will not be exactly straight under these circumstances as for dams on a level terrain but this is a reasonable local approximation at each point along the shock because the shock angle is in practice close to the deflecting angle for deflecting dams that need to be considered in practice. The dynamic effect of variations in the downstream flow depth, h_2, with distance along the dam is, furthermore, neglected here.

The geometry of the shock along the dam in the moving frame of reference leads to the

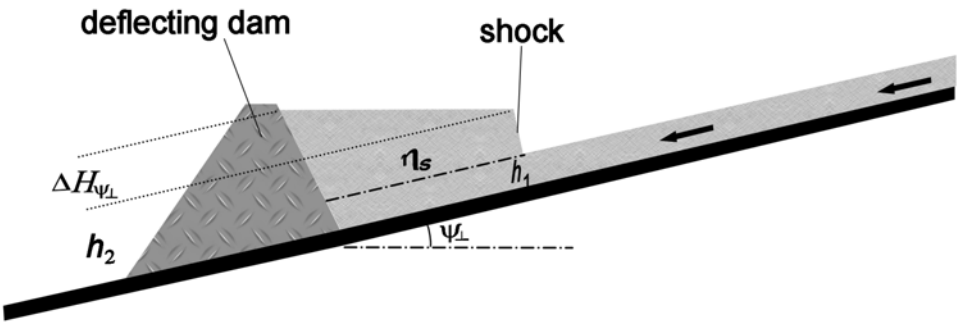

Figure 16: Schematic cross section of a shock formed along a deflecting dam built on terrain sloping towards the dam. In a coordinate system moving with the avalanche along the dam, the shock is propagating away from the dam with speed c. Material flows across the shock and forms a horizontal surface in the direction normal to the dam axis. $\psi_\perp$ is the slope of the terrain in the direction normal to the dam axis and η_s is the width of the shock.

following expression for the propagation speed of the shock, c, away from the dam

$$c = \frac{u_1 h_1}{e(h_2 + \eta_s \tan\psi_\perp) - h_1} \,, \tag{28}$$

where η_s is the width of the shock in the direction normal to the dam axis (see Fig. 3), $\psi_\perp$ is the terrain slope towards the dam, and e is a geometrical factor given by

$$e = (1 + \cos\alpha \sin\psi_\perp / \sin(\alpha - \psi_\perp)) \,. \tag{29}$$

This leads to the following shock relation

$$(h_2/h_1)^2 - (h_2/h_1) - 2\mathrm{Fr}_\perp^2 \left(\frac{e(h_2 + \eta_s \tan\psi_\perp)}{e(h_2 + \eta_s \tan\psi_\perp) - h_1} \right)^2 = 0 \,, \tag{30}$$

which determines the shock height h_2 at a given distance away from the dam. In general, Equations (28) and (30) must be solved as a coupled set of equations for η_s and h_2, but an approximate solution is sufficient for our purposes here.

When there is no terrain slope towards the dam, the distance of the shock from the dam is $\eta_s = \tan(\theta - \varphi)\,\xi \approx \sqrt{2}/(2\,\mathrm{Fr}\cos\varphi)\,\xi$, where ξ is distance along the dam from its upstream end and the approximate expression for the shock widening $(\theta - \varphi)$, correct to $O(\mathrm{Fr}^{-2})$, is from Hákonardóttir and Hogg (2005). This width is an upper bound on the shock width for dams on a sloping terrain because the effect of the slope towards the dam is to narrow the shock. The shock height given by (30) may, furthermore, be shown to be comparatively unaffected by the slope towards the dam relative to the shock height given by (19). Neglecting a small effect due to the slope of the upstream dam face, these approximations may be used to express an approximate upper bound on the extra run-up on the dam side (normal to the terrain) as

$$\Delta H_{\psi_\perp} = \tan\psi_\perp \, \eta_s = \frac{\sqrt{2}\tan\psi_\perp}{2\,\mathrm{Fr}\cos\varphi}\,\xi \,. \tag{31}$$

The increased dam height specified by (31) is in most cases not appreciable, but it needs to be taken into account in rare cases when $\psi_\perp > 5^\circ$, especially if the flow depth is large or the velocity rather low so that the Froude number is low.

11 Curvature of the dam axis: ΔH_κ

The analysis has so far been based on the simple geometry of a straight dam that is hit by a flow with uniform thickness and velocity. Avalanche dams frequently need to be curved along the dam axis in order to protect as large an area as possible. The curvature of the dam axis then affects the run-up of the avalanche due to the centripetal acceleration that is introduced as the flow bends around the curved dam geometry (Fig. 17). The run-up requirement derived from supercritical overflow is not affected by the curvature of the dam axis because the question of overflow is settled based on the local dam height and deflecting angle at each point along the dam axis. As for terrain slope towards the dam discussed in Section 10, the run-up height corresponding to the flow depth downstream of a shock along the dam needs to be reconsidered when the dam is curved, but not the run-up height corresponding to supercritical overflow.

Assuming that the centripetal acceleration is counteracted by a slope of the surface of the flow away from the dam over the width of the shock that has been formed along the dam, the extra run-up on the dam side that needs to be taken into account is given by

$$\Delta H_\kappa = \frac{(u_1 \cos\varphi)^2}{g \cos(\psi) R_\kappa} \eta_s = \frac{\sqrt{2}\,(u_1 \cos\varphi)^2}{2\,\mathrm{Fr} \cos(\varphi)\, g \cos(\psi) R_\kappa} \xi\,, \tag{32}$$

where g is the acceleration of gravity, R_κ is the radius of curvature of the dam axis, η_s is the width of the shock in the direction normal to the dam axis and ξ is distance along the dam axis from its upstream end. The same approximations have been used to express the width of the shock as in the preceding section about terrain slope towards the dam.

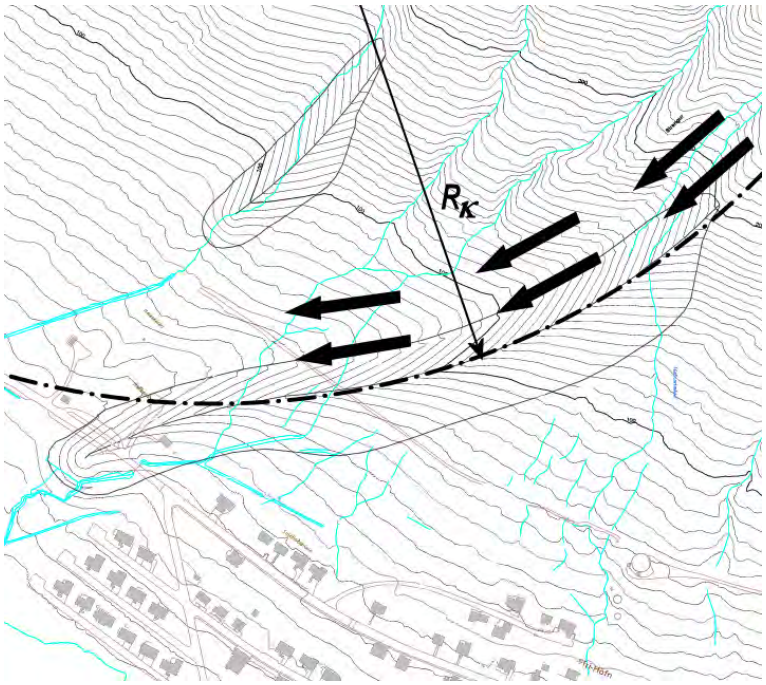

Figure 17: The deflection of an avalanche alongside the ≈700 m long, curved deflecting dam below Ytra-Strengsgil in Siglufjörður, northern Iceland. A circle with a radius of curvature $R_\kappa \approx 700$ m has been fitted to the curved dam axis. In this case, the assumed design avalanche ($u_1 = 40$–$45\,\mathrm{ms}^{-1}$, $h_1 = 6$–8 m) leads to a significant run-up contribution $R_\kappa \approx 9$ m due to the curvature of the dam at the downstream end of inflow from the gully towards the dam.

Avalanches hitting curved deflecting dams often flow out of gullies or confined avalanche paths where the flow towards the dam has a limited width. The deflecting dam may, however, extend out of the avalanche stream to divert the avalanche flow away from an area that needs to be protected. In such cases, the length ξ along the dam in Equation (32) only needs to be considered up to a maximum value corresponding to the distance along the dam where there is flow towards the dam upstream of the shock (see Fig. 17). Beyond this point, the maximum value of ξ and the corresponding distance of the shock from the dam, η_s, may be used all the way to the downstream end of the dam.

The simple derivations presented here and in the preceding section to take into account dam curvature and the slope of the terrain towards the dam are sometimes inappropriate when dam and terrain geometry are complex. In such cases, it is advisable to use 2D avalanche modelling with a shock capturing algorithm to investigate these effects in more detail, possibly with guidance from the simple results presented here.

12 Lateral spreading of the flow below the downstream end of the dam

Snow avalanches will spread out laterally when they flow past deflecting dams. In some cases, particularly for wet-snow avalanches, an avalanche or the part of an avalanche may turn abruptly when it flows past the end of a dam, but in other cases, the avalanche may continue in the direction of the dam axis and almost no spreading of the flow downstream of the dam can be seen.

The spreading of granular materials when the lateral constraints provided by a dam come to an end has been analysed analytically based on shallow fluid theory by (Hogg and others, 2005). This theory predicts that the maximum lateral spreading (in terms of the angular width of a fan beyond the dam axis formed at the downstream end of the dam) is a decreasing function of the Froude number of the flow and is approximately given by

$$\phi_{\mathrm{lsp}} = \frac{2}{\mathrm{Fr}} - \frac{5}{3\,\mathrm{Fr}^3} + O\left(\frac{1}{\mathrm{Fr}^5}\right) . \tag{33}$$

The theory predicts a spreading of 11–21° for Fr in the range 5–10, which is not inconsistent with a value of 20° that has sometimes been adopted in Switzerland for this type of widening (Stefan Margreth, personal communication 2006). It should be noted that smaller and slower avalanches than the design avalanche may need to be taken into account when the effect of this widening below the dam is considered because such avalanches are predicted to form a wider fan than larger and faster avalanches. As noted above, wet-snow avalanches may make much sharper turns around dam ends than dry-snow avalanches so this estimate cannot be used for dams intended as protection against such avalanches.

13 Storage above a catching dam: S

There must be sufficient space above a catching dam to store the volume of snow corresponding to the deposit of the design avalanche, which is successfully stopped by the dam. According to traditional dam design principles in Switzerland and some other countries (Margreth, 2004), the storage space per unit width above a catching dam is computed as the area between the snow covered terrain and a line from the top of the dam with a slope of 5–10° away from the mountain (see Fig. 18). This requirement is primarily intended for slow, moist, dense avalanches (see Fig. 19) and the storage capacity for fast, dry-snow avalanches can be much smaller. A compaction factor of approximately 1.5, describing the ratio of deposit density to release density is, furthermore, sometimes used (Stefan Margreth, personal communication 2006). In some cases, the storage space above a catching dam must be dimensioned so that more than one avalanche per season can be stopped by the dam. This procedure for designing the storage space is not based on any dynamical principles and it is, therefore, not consistent with the overall framework described in the previous sections for determining the dam height.

Catching dams are usually built in the run-out zone of avalanches where terrain slope may be expected to be smaller than the internal friction angle of avalanching snow, ϕ, which is, however, not well known and likely depend on the type of snow. In this case, one may expect a shock propagating upstream from the dam to maintain its thickness away from the dam (see Hákonardóttir, 2004), even when the terrain slopes towards the dam. There is, however, considerable uncertainty regarding the propagation of the shock over possibly uneven terrain. The storage volume computed from shock dynamics in this manner would, for many dams on sloping terrain, be larger than the volume found with the traditional procedure, because the deposit thickness would not be reduced much with distance away from the dam.

Observations from the catching dam at Ryggfonn indicate that dry-snow avalanches do not pile much up against the dam so that the avalanche deposits slope in many case away from the dam rather than towards the dam.

In the absence of a better choice, it is proposed here to continue to use the traditional methodology, with a deposit slope of 0–10° (see Fig. 18), and without a compaction factor. The storage volume may then be found from the equation

$$S = \int_{x_0}^{x_1} (z_l - (z_s + h_s))dx \,, \tag{34}$$

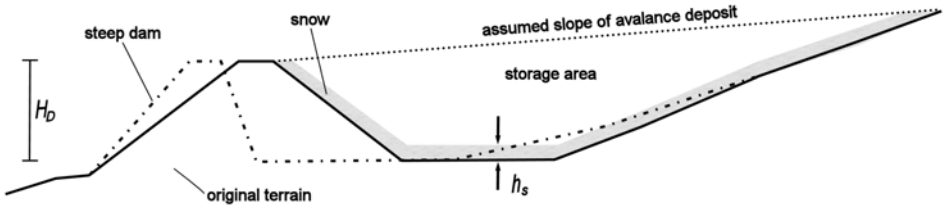

Figure 18: Schematic figure of the snow storage space above a catching dam. h_s is the thickness of snow and previous avalanche deposits on the ground on the upstream side of the dam before an avalanche hits the dam. H_D is the vertical height of the upstream dam side. The figure is adapted from Margreth (2004).

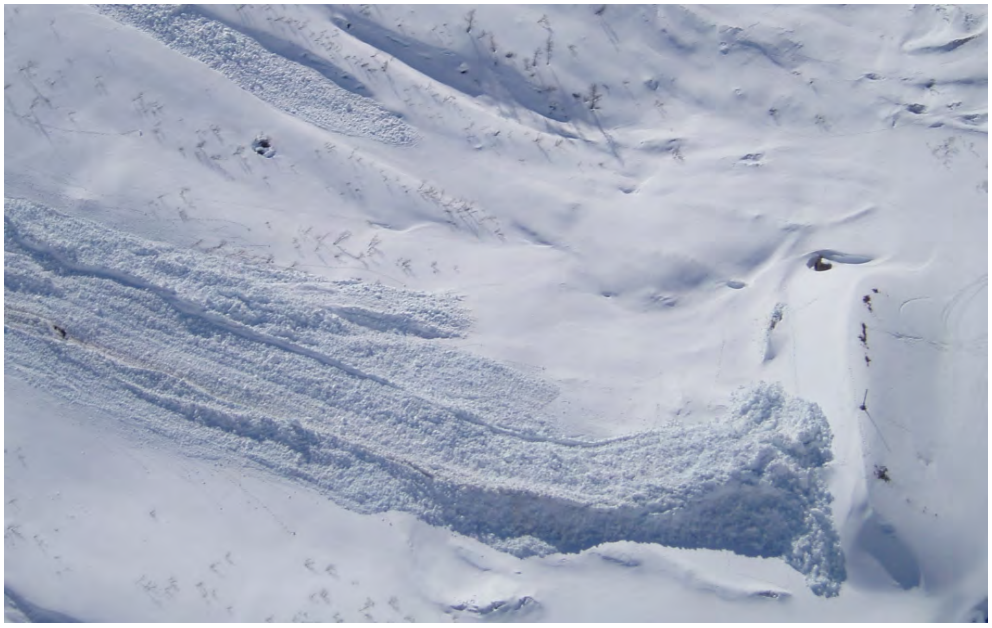

Figure 19: A wet-snow avalanche stopped by a catching dam in Ryggfonn, western Norway, on 16 April 2005, photograph: NGI.

where x is horizontal distance from the dam, z_l is the elevation of a straight line from the top of the dam towards the mountain with a chosen slope in the range 0–10°, $z_s + h_s$ is the elevation of the top of the snow cover before the avalanche falls, and x_0 and x_1 are the locations of the dam and the point where the line intersects the snow covered mountainside, respectively. For dams where dry-snow avalanches are expected, deposit slopes close to 0° should be used, but for locations where wetter avalanches are typical slopes up to 10° can be chosen. This procedure is not very satisfactory because it is not based on dynamic principles and needs to be refined in the future by further studies.

14 Comparison of the proposed criteria with observations of natural avalanches that have hit dams or other obstacles

This section summarises available data about run-up of snow avalanches on natural and man-made obstacles and compares them with the design criteria proposed here. The measured run-up together with data characterising the avalanches and their paths are tabulated in Table 1. The observed run-up was plotted together with theoretically predicted run-up ranges in Figure 13 in the previous section about momentum loss in the impact with an obstacle. The flow depth, h_1, and velocity, u_1, of the oncoming flow are the most important parameters determining the predicted run-up, but they are unknown for all the avalanches. The velocity was estimated by modelling the avalanche flow with several different avalanche models. The flow depth was estimated subjectively, with some assistance from the modelling for a few of the avalanches. The uncertainty of u_1 is somewhat arbitrarily assumed to be $\pm 15\%$ and h_1 is most often assumed to lie in the range 1–3 m. Snow depth on the terrain before the avalanches fell, h_s, is not taken into account in the derivation of the theoretical run-up ranges. As h_s may be expected to be substantially smaller than the observed run-up, this should not make much difference for the interpretation of the results.

Run-up of natural avalanche on obstacles is traditionally measured in a vertical cross section normal to the dam or obstacle axis in the map plane. This is the run-up that is most easily measured in the field or on a map showing run-up marks that have been identified in the terrain and positioned with geodetic instruments. In order to compare data on vertical run-up of natural avalanches with the theory developed here, one must transform the theoretically derived run-up normal to the upstream terrain, h_r, to vertical run-up, r. It is also often necessary to transform deflecting angles measured in the horizontal map plane, φ_h, to deflecting angles in a sloping plane aligned with the terrain, φ (see Fig. 2), which are used in run-up formulae derived here. Formulae for carrying out these transformations and some related formulae that are useful in the analysis of run-up data are given below for completeness.

The deflecting angle in the sloping plane, φ, may be computed from the deflecting angle measured on a map, φ_h, and the slope of the upstream terrain, ψ, with the formula

$$\tan\varphi = \tan\varphi_h \cos\psi \,. \tag{35}$$

Terrain slope in the direction normal to the dam axis, $\psi_\perp$, is given by

$$\sin\psi_\perp = \sin\varphi \sin\psi \,. \tag{36}$$

Vertical run-up, r, can be computed from the run-up normal to the upstream terrain, h_r, according to

$$r = \frac{\cos\psi - \sin\varphi \sin\psi \cot\alpha}{1 - \cos^2\varphi \sin^2\psi}\, h_r \,, \tag{37}$$

where α is the angle of the dam side with respect to the terrain in the direction normal to the dam axis in a plane normal to the upstream terrain (see Fig. 2 for a geometrical explanation of the angles used in this equation). The steepest inclination of the dam or the upstream facing side of the obstacle, α_s, satisfies the equation (see Domaas and Harbitz, 1998)

$$\sin^2\alpha_s = (\cos\varphi \sin\psi)^2 + (\cos\psi \sin\alpha - \sin\varphi \sin\psi \cos\alpha)^2 \,, \tag{38}$$

from which α may be found using

$$\sin^2(\alpha-\gamma) = \frac{\sin^2\alpha_s - \cos^2\varphi\sin^2\psi}{\cos^2\psi + \sin^2\varphi\sin^2\psi}\,, \tag{39}$$

where $\tan\gamma = \sin\varphi\tan\psi$. Finally, the deflecting angle, φ, sometimes needs to be found from the measured angle, φ_c, between the direction of the avalanche and contour lines of the opposing slope in the map plane using the formula

$$\tan\varphi_c = \frac{\sin\varphi\cos\psi\sin\alpha - \sin\psi\cos\alpha}{\cos\varphi\sin\alpha}\,. \tag{40}$$

The above formulae were used to derive an internally consistent set of slopes, deflecting angles and run-up for comparing measured vertical run-up with the theoretical run-up estimates normal to the terrain derived here. These data were already presented above in Figure 13 as a part of the discussion of the loss of momentum in the impact with an obstacle, but they will now be described and discussed in more detail.

Avalanches hitting natural deflecting dams in Norway

Information about 15 avalanches from Norway that have hit terrain obstacles or man-made dams was obtained from Harbitz and Domaas (1997), Domaas and Harbitz (1998) and Harbitz and others (2001). The original information has been rechecked and some minor corrections have been made as described in Harbitz and Domaas (in prep.). The avalanches have estimated volumes ranging from about 15 thousand m^3 to 250 thousand m^3, and modelled impact velocities in the range 20–60 ms^{-1}. The vertical run-up ranges from 7 to 90 m. Two of the avalanches hit man-made dams and all the other avalanches hit natural obstacles. Some of the avalanches, such as the Tomasjorddalen, Vassdalen and Gaukheidalen avalanches, hit obstacles that have a simple geometry quite similar in form to man-made dams. Others are less suitable for validation of the theoretical run-up expressions, which are being analysed here. The upstream velocity of the Norwegian avalanches was estimated with the PCM model by choosing model parameters that reproduced the observed run-out of the avalanches and based on experience with this model at NGI (Harbitz and Domaas, in prep.). The upstream flow depth was in most cases (subjectively) assumed to lie in the range 1–3 m. A slightly larger flow depth was adopted for the three largest avalanches and a slightly smaller upper limit for the flow depth was chosen for the four smallest avalanches. The run-up height is in some cases estimated based on damages to forest which could be caused by the powder cloud component of the avalanche in which case the height would be an overestimate of the run-up of the dense core. This applies to the Åpoldi-G, Åpoldi-L and Tomasjorddalen avalanches.

Flateyri, Iceland, 1995

The catastrophic avalanche at Flateyri in 1995, which killed 24 persons, changed direction when it entered a gully in the middle of its path. The run-up was judged from marks left on the terrain by boulders, which were advected in large quantities with the avalanche (Þorsteinn Sæmundsson, personal communication). The run-up marks indicate a vertical run-up of approximately 20 m at the location of impact with the gully side at approximately 400 m a.s.l.,

but this must be considered rather uncertain as the run-up marks were not easy to identify at this location (they were easier to identify farther down the track). However, it is clear that the avalanche did not overflow the downstream side of gully, which provides a definite upper bound of 30–40 m on the vertical run-up. The upstream velocity and flow depth of the avalanche were modelled with the SAMOS model (Zwinger and others, 2003). The impact of this avalanche with the gully wall at a deflecting angle of approximately 30° provides important evidence that deflecting dams work roughly in accordance with theory for very large avalanches at rather high deflecting angles.

Flateyri, Iceland, 1999 and 2000

Two avalanches with volume on the order of 100 thousand m^3 have hit the deflecting dams at Flateyri in northwestern Iceland (Jóhannesson, 2001). The dams have a simple geometry, which is similar to the simplified geometry assumed in the theoretical analysis presented here (see Fig. 2). For this reason, they should be suitable for validating the theory. However, the run-up marks were identified on loose snow on the dam sides and they may, therefore, partly be formed by the saltation layer of the avalanche rather than by the dense core. The run-up of these avalanches, thus, provides an upper bound on the run-up, but it is uncertain how high on the dams the top of the dense core reached. The upstream velocity and flow depth of this avalanche were modelled with the SAMOS and MN2D depth-averaged, two-dimensional avalanche models (Zwinger and others, 2003; Mohamed Naaim, personal communication 2006). Based on the deposit thickness and on the model results, an upstream flow depth h_1 =1–2 m was assumed near the dams for both avalanches.

Kisárdalur, Iceland, 1995

The Kisárdalur avalanche in Fnjóskadalur in northern Iceland fell in the Flateyri avalanche cycle in 1995. It completely overflowed an approximately 60 m high ridge, without leaving much snow in the gully at the bottom of the ridge, and continued some 250 m beyond the top of the ridge. The upstream velocity and flow depth of this avalanche was modelled with the SAMOS avalanche model using similar initial conditions as for the SAMOS modelling of the Flateyri 1995 avalanche since it fell in the same avalanche cycle. The simulation indicates a strong channelisation and large flow depth of the avalanche in a gully leading up to the impact with the ridge. Based on the model results, a flow depth of approximately 10 m was assumed at the foot of the ridge.

Taconnaz, France, 1999

The avalanche at Taconnaz in France in 1999 is the largest avalanche in the data set with an estimated volume of 700–800 thousand m^3. It hit three obstacles on its way down the lower part of the approximately 6 km long Taconnaz path and, thus, provides three of the data points about run-up in Figure 13. First it hit an approximately 60 m high glacier moraine at a deflecting angle of approximately 40° at a very high velocity, which is here estimated to have been on the order of 70 ms^{-1}, apparently without overtopping. Earlier avalanches in the same path have, however, slightly overtopped this moraine (Francois Rapin, personal communication 2006). Therefore, this avalanche is marked in Table 1 and Figure 13 as having nearly

overflowed the moraine. Farther down the path, the same avalanche overflowed both a 10 m high deflecting dam and a 15 m high catching dam. The information about this avalanche was obtained from the records of Cemagref in Grenoble (Mohamed Naaim and Francois Rapin, personal communication 2006). The upstream velocity and flow depth of the avalanche at the dams were modelled with the MN2D depth-averaged, two-dimensional avalanche model (Mohamed Naaim, personal communication 2006). Based on the model results, a flow depth of 4–8 m was assumed near the glacier moraine, 5–8.5 m near the upper dam and 3–4.5 m near the lower dam.

The data set

Table 1 lists the measured run-up of each of the 22 avalanches in the data set together with data characterising the avalanches and the paths. The flow depth, h_1, is given as a range as described in the previous subsections about the avalanches. The velocity, u_1, is given as a single value but assigned an uncertainty of $\pm 15\%$ in Figure 13 and in the discussion below.

Interpretation

Several interesting features are evident from the data shown in Table 1 and Figure 13. The most disconcerting aspect of the figure is that three of the Norwegian avalanches (Åpoldi-G, Lillestølsætra and Vassdalen) and one of the Icelandic avalanches (Kisárdalur) have run-ups that are substantially higher than can be reconciled with the proposed design criteria. Although the Kisárdalur avalanche is near the upper limit of the theoretical range, the fact that it overflowed the obstacle almost completely and continued another 250 m down the slope indicates that the run-up and overflow in combination are hard to reconcile with the theoretical predictions. In addition, the Langageiti avalanche slightly overflowed an 11 m high dam for which the upper limit of the predicted ranges is about 8.5 m, and the Legdefonna avalanche produced 10 m high run-up marks where the upper limit of the ranges is about 6.5 m. Two of the Icelandic avalanches on the deflecting dams at Flateyri (Flateyri, Skollahvilft, 1999, and Flateyri, Innra-Bæjargil, 2000) also have run-ups in excess of the ranges predicted by the design expressions, but this may, as mentioned above, perhaps be explained by the run-up marks on loose snow on the dam sides being caused by the saltation layer of the avalanche rather than by the dense core. Two Norwegian avalanches, which clearly overflowed the obstacle, apparently without much deflection (Årsæterstøylen and Storegjølet), are well below the theoretical ranges so this overflow is not unexpected. The remaining 12 avalanches are within or near the ranges corresponding to the higher one of the proposed criteria, except for one of the Norwegian avalanches (Indre-Standal-L), which is within the lower range.

The excess run-up of the Langageiti and Legdefonna avalanches may be related to the very steep terrain ($\psi > 35^\circ$) where the dam/obstacle is located in these cases. The assumption that the downslope component of the gravitational acceleration is approximately balanced by friction may then not be justified. The angle of the obstacle with respect to the sloping terrain, α, is, furthermore, rather slight (24°) for the Legdefonna obstacle, which leads to a large difference between run-up height normal to the terrain (h_r) compared with vertical run-up (r). These two avalanches indicate that the proposed dam design criteria need to be applied with caution in very steep terrain, and possibly supplemented with 2D numerical modelling where the effect of gravity and friction can be treated more satisfactorily.

Path	z_o	z_s	ψ	$\psi_\perp$	φ	φ_h	α_s	α	h_{1_i}	h_{1_x}	u_1	V_o	V_s	r	O	L
Norwegian avalanches																
Åpoldi-G	1300	0	21.8	12.7	36.4	38.5	59	70.7	2	4	31.8	80	250	44.1	f	T
Åpoldi-L	1300	0	21.8	17.4	53.7	55.7	41.6	57.8	2	4	31.8	80	250	19.7	f	F
Tomasjorddalen	1100	0	21	17.5	56.9	58.7	49	65.8	1	3	51.1	60	200	90	F	F
Årsæterstøylen	1000	220	18.4	12.5	43.5	45	37	47.8	2	5	43.1	50	150	11.8	T	T
Lillestølsætra	800	195	12.5	8.9	45.8	46.5	18.4	25.2	1	3	32.3	30	100	43.9	F	F
Vassdalen	470	210	26.5	16.7	40	43.2	33	44.6	1	3	28	6	12	25	F	F
Legdefonna	1400	420	38.3	13.8	22.6	27.9	35.5	23.8	1	3	38.5	40	100	10	f	F
Indre-Standal-U	1300	0	29	18.4	40.7	44.5	46	61.8	1	3	40.4	30	50	11.9	F	T
Indre-Standal-L	1300	0	8.8	7.7	60.7	61	20.3	27.5	1	3	23	30	50	8.4	f	F
Storegjølet	1000	120	20.5	16.3	53.2	55	41.4	56.6	1	3	59.1	25	50	8	T	T
Saurasetra	600	375	18.4	8.2	27	28.2	29.7	33.7	1	3	33.5	10	20	12.5	T	F
Gaukheidalen	375	50	21.8	9	24.9	26.6	36	40.3	1	2	34.5	7	15	8.7	F	T
Drevja	700	20	36	33.6	70.2	73.8	30	62.3	1	3	47.5	NA	150	30	T	T
Nautagrovi	1380	0	22	12.1	34	36	39	47.9	1	2	20	NA	100	7	F	T
Langageiti	1300	0	36	17.1	30	35.5	39	45.4	1	2	27	NA	60	11	f	T
Icelandic avalanches																
Kisárdalur-1995	680	355	23	22.5	78.4	79.3	36	58.3	8	12	45	35	70	60	T	T
Flateyri-1995	660	0	36	17.3	30.4	35.9	38.7	45.3	3	7	44	280	430	20	F	T
FlateyriSkh-1999	660	0	9.5	2.9	18	18.2	40	42.1	1	2	30	54	130	13	F	T
FlateyriIBg-2000	660	0	13	5.5	25	25.6	40	44.1	1	2	30	44	110	12	F	T
The Taconnaz avalanche																
TaconnazGM-1999	4000	1010	34	20.9	39.7	45	35	48.1	4	8	70	NA	800	60	f	T
TaconnazDD-1999	4000	1010	13	0	30	30.6	35	40	5	8.5	25	NA	800	10	T	T
TaconnazCD-1999	4000	1010	11	11	90	90	70	81	3	4.5	15	NA	800	15	T	T

Table 1: Run-up of snow avalanches from Norway, Iceland and France. See the "Notation" section for explanations of most of the variables. The columns z_o and z_s give the starting and stopping altitudes of the avalanches. h_{1_i} and h_{1_x} are the minimum and maximum estimated flow depth. V_o and V_s are rough estimates of the volume released from the starting zone and the total volume including entrainment along the path. The column labelled "O" specifies whether a substantial part or the entire avalanche overflowed the obstacle ("T"), overflowed the obstacle slightly ("f"), or did not overflow ("F"). The column labelled "L" specifies whether the path has an abrupt change in slope at the foot of the obstacle so that momentum loss in the impact with the obstacle is assumed ("T") or not ("F"). The table contains both deflecting obstacles and obstacles that are more or less normal to the flow direction as a catching dam (Åpoldi-L, Tomasjorddalen, Indre-Standal-L, Storegjølet, Drevja, Kisárdalur and TaconnazCD have $\varphi > 50°$). Note that the run-up marks may in some cases have been caused by the saltation or powder parts of the avalanches in which case the tabulated run-up height would an overestimate of the run-up of the dense core (this applies in particular to the Åpoldi-G, Åpoldi-L, Tomasjorddalen and Flateyri 1999 and 2000 avalanches).

Three of the Norwegian avalanches (Åpoldi-G, Lillestølsætra and Vassdalen) stand out with very high run-up relative to the theoretical derivations (a difference by a factor on the order of 2). As mentioned before, the highest run-up marks produced by the Åpoldi-G avalanche are likely to have been produced by the powder part of the avalanche in which case the observed run-up would be an overestimate of the run-up of the dense core. Nevertheless, the run-up does not compare well with the proposed criteria. The paths of the Lillestølsætra and Vassdalen avalanches have rather smooth transitions between the mountainside and the obstacle so that the avalanches are able to flow up on the obstacle without an abrupt change in flow direction. The Kisárdalur avalanche from Iceland, on the other hand, completely overflowed an approximately 60 m high opposing slope, which is almost normal to the oncoming flow direction and meets the upstream mountainside in a rather sharp corner in a gully.

Figure 13 shows nicely how supercritical overflow is the more important overflow mechanism for the higher normal velocities, but for lower normal velocities, flow depth downstream of a shock becomes more important. An analysis of run-up based only on supercritical overflow (or on the traditional run-up expressions (1) and (2)) may, therefore, produce a misleading relationship between run-up and normal velocity. The figure shows that the upstream flow depth, h_1, has little effect on the run-up predicted by supercritical overflow except at low normal velocities (the thick red arrows are very short except near the left end of the figure).

On the positive side, Figure 13 shows that the run-up marks of several medium-sized and large avalanches are in rough agreement with the proposed criteria, and that the overall variation of the run-up with normal velocity is in general agreement with the criteria (except of course for the four abovementioned avalanches with higher run-up and the avalanches at Flateyri in 1999 and 2000). The avalanche at Taconnaz in France in 1999 represents important data points. It *did not overflow* the approximately 60 m high glacier moraine, as evidenced by the symbol in Figure 13 near the upper limit of the range corresponding to supercritical overflow for momentum loss in the impact. This interpretation of the Taconnaz event indicates that the validity of the criteria is not limited to low speeds or acute deflecting angles, or to small laboratory scales and only the granular materials that were used in the laboratory experiments. Farther down the path, the Taconnaz avalanche *overflowed* a 10 m high deflecting dam and a 15 m high catching dam, which is shown with two symbols in Figure 13 that fall well within the theoretically predicted ranges. The location of the symbols corresponding to the three events at Taconnaz in Figure 13 with respect to the theoretically predicted ranges indicates that the theory does not systematically underestimate or overestimate run-up.

The high observed run-up of some of the avalanches does, however, indicate a larger uncertainty in the estimated velocity than assumed here, or some run-up mechanism that is not accounted for in the theoretical analysis. Some of the highest run-up marks may, as mentioned above, be caused by the impact of the saltation or powder components of the avalanches, which may, for example, damage forest considerably higher up than the highest point reached by the dense core. Pressure from the saltation or powder layers can, however, not account for the complete overflow of the Kisárdalur avalanche, which left very little snow in the gully at the foot of the obstacle. These events need to be taken as reminders of the imperfect dynamic basis of the proposed run-up criteria, indicating that natural avalanches are perhaps of several different types, which are not adequately described by a single dynamic framework. In spite of the problems indicated by the partial agreement between the run-up data and the new design criteria, these criteria are proposed here as a substantial improvement over traditional criteria.

15 Unresolved issues

Several issues need to be further investigated in order to improve avalanche dam design criteria beyond the guidelines proposed here. The most important issues that must be addressed are listed below.

Loss of momentum in the impact with the dam. The proposed values of the k-factor (Eq. (27)) are based on weak arguments. In particular, new analysis of data about dam overflow from the full-scale Ryggfonn test site in Norway (NGI, 2005) indicates that very little energy loss occurs above a dam with a side slope of about 40°. These results may be interpreted as an indication that loss of kinetic energy in the impact with the dam, for avalanches that overflow, equals *on the order of half the potential energy corresponding to the freeboard of the dam*. This means that λ is on the order of 0.5 in this case, rather than 1.5, as proposed here! These results are very disconcerting and need to be analysed further. They may indicate the lack of some fundamental dynamic process in the analysis of overflow, which is summarised in this report. Observations of run-up marks on natural obstacles for real snow-avalanches indicate, however, that much more energy than this is lost in impacts of avalanches with abrupt obstacles. Run-up marks and data about avalanche overrun need to be analysed further to resolve this discrepancy.

The maximum deflecting angle φ_{max}. The requirement that φ is at least 10° smaller than φ_{max} needs to be discussed further. Is the rather arbitrary value of 10° appropriate or should some other value be chosen?

Effect of terrain slope towards the dam on the shock height. Hydraulic jumps in fluid flow in sloping channels are affected by the channel slope, which leads to an increase in flow depth downstream of the jump for positive slopes (see Chow, 1959). This effect, which arises from the action of the gravitational force over length of the jump, can be taken into account by an adjustment of the Froude number based on empirical data about water flows. However, granular jumps have been observed to be considerably shorter than water jumps (see Hákonardóttir, 2004), and the gravitational force is here assumed to be to a large extent balanced by frictional forces in shocks that are formed above avalanche dams. Therefore, it is not clear to what extent this effect of terrain slope should be taken into account in design criteria for avalanche dams. If dams are constructed in areas where the avalanches may be expected to be slowing down, one might even argue that this is equivalent to fluid flow in an up-sloping channel, where this effect acts in the opposite direction.

Effect of entrainment and deposition. Deposition may be an important process when an avalanche hits a dam and entrainment can possibly have an effect under some circumstances but these effects have been neglected here.

Effect of the saltation and powder parts. A major limitation of the dynamic description of the impact process developed here results from the depth-averaged formulation of the shallow flow of the dense core of the avalanche. As a consequence, the saltation and powder components are ignored. These components may lead to important overflow in some cases and they may cause substantial impact on structures below the dam, which

cannot be evaluated based on the simplified dynamic framework. This limitation needs to be addressed in further studies.

16 Conclusions

The dam height criteria suggested here are derived from an internally consistent description of the dynamics of the flow of snow avalanches against obstacles based on shallow fluid dynamics. In that respect, they are a step forward from traditional criteria based on point-mass dynamics that are not consistent with the avalanche body having non-zero width or length.

The new criteria are based on two separate requirements. Firstly, uninterrupted, supercritical flow over the dam must be prevented, and, secondly, the dam must be higher than the flow depth below an oblique or a normal shock that may form upstream of the dam. An avalanche dam must be higher than the maximum of the two requirements. A set of geometrical transformations makes it possible to adapt the requirements to dams that need to be built on sloping terrain.

In spite of the advance provided by the depth-averaged, shallow fluid dynamics, the proposed dam height criteria can only be partially reconciled with field evidence about the run-up of avalanches against dams and natural obstacles. Many avalanches produced run-up marks that are in reasonable agreement with the theoretical preductions. Several avalanches have, however, produced higher run-up marks or overflowed higher obstacles than predicted by the theory, indicating a large uncertainty in the estimated impact velocity, or a run-up mechanism that is not accounted for in the theoretical analysis.

17 Acknowledgements

This study was carried out with support from the European Commission (the research project *SATSIE*, grant EVG1-CT-2002-00059), and the Icelandic Avalanche Fund. Support for studying run-up of Norwegian avalanches on terrain obstacles was provided by a grant from the Norwegian Ministry of Industry and Energy for the project “581210 Utløpsdistance (run-out distance)” at NGI.

18 References

Chapman, C. J. 2000. *High Speed Flow*. Cambridge texts in applied mathematics. Cambridge University Press, UK.

Chow, V. T. 1959. *Open-channel hydraulics*. McGraw-Hill Inc.

Chu, T., G. Hill, D. M. McClung, R. Ngun and R. Sherkat. 1995. Experiments on granular flow to predict avalanche runup. *Canadian Geotechnical Journal*, **32**, 285–295.

Domaas, U., and C. B. Harbitz. 1998. On avalanche run-up heights on deflecting dams: Centre-of-mass computations compared to observations. *In*: Hestnes, E., *ed.*, *25 years of snow avalanche research*. Oslo, NGI, Publikation nr. 203, 94–98. Revised version in NGI Report 581210-4, 1999.

Gauer, P., and K. Kristensen. 2005. *Avalanche studies and model validation in Europe, SATSIE; Ryggfonn measurements: Overview and dam interaction*. Oslo, Norwegian Geotechnical Institute, Rep. 20021048-10.

Gray J. M. N. T., Y.-C. Tai and S. Noelle. 2003. Shock waves, dead-zones and particle-free regions in rapid granular free surface flows. *J. Fluid Mech*, **491**, 161–181.

Hager, W. H., 1992. *Energy Dissipators and Hydraulic Jump*. Dordrecht, Kluwer Academic Publishers.

Harbitz, C. B., and U. Domaas. 1997. *Run-out distance: Mapping of natural deflecting dams*. Oslo, NGI, Report 581210-1.

Harbitz, C. B., and U. Domaas. (in preparation). *Mapping of natural deflecting dams and application of a centre-of-mass model*. Oslo, NGI, Report 581210-2.

Harbitz, C. B., U. Domaas and A. Engen. 2001. *Design of snow avalanche deflecting dams*. Oslo, NGI, Report 589000-4. Also in: *Proceedings of the 9th Interpraevent 2000 Congress, 26th – 30th June 2000*, Villach, Austria, **1**, 383–396.

Hákonardóttir, K. M. 2004. *The interaction between snow avalanches and dams.* University of Bristol, School of Mathematics (PhD thesis).

Hákonardóttir, K. M., A. J. Hogg, T. Jóhannesson and G. G. Tómasson. 2003. A laboratory study of the retarding effects of braking mounds on snow avalanches. *J. Glaciol.*, **49**(165), 191–200.

Hákonardóttir, K. M., and A. J. Hogg. 2005. Oblique shocks in rapid granular flows. *Physics of Fluids*, **17**, 077101, doi:10.1063/1.1950688.

Issler, D. 2003. Experimental information on the dynamics of dry-snow avalanches. *In*: Hutter, K. and N. Kirchner (eds.), *Dynamic Response of Granular and Porous Materials under Large and Catastrophic Deformations*. Berlin, Springer, Lecture Notes in Applied and Computational Mechanics, **17**, 109–160.

Hogg, A. J., J. M. N. T. Gray and X. Cui. 2005. Granular vacua. *In*: Carcia-Rojo, R., H. J. Herrmann and S. McNamara (eds.), *Powders and grains 2005*. Rotterdam, A. A. Balkema, 929–933.

Hungr, O., and D. M. McClung. 1987. An equation for calculating snow avalanche run-up against barriers. *In: Avalanche formation, movement and effects (Proceedings of the Davos Symposium, September 1986)*, IAHS Publ. **162**, 605–612.

Jóhannesson, T. 2001. Run-up of two avalanches on the deflecting dams at Flateyri, northwestern Iceland. *A. Glaciol.*, **32**, 350–354.

Margreth, S. 2004. Avalanche control structures. *In: Pôle Grenoblois d'Etudes et de Recherche pour la Prévention des Risques Naturels. UEE session 2004: avalanches : risque,*

zonage et protections, Courmayeur.

Takahashi, T. and H. Yoshida. 1979. *Study on the deposition of debris flows, Part I—Deposition due to abrupt change of bed slope*. Kyoto University, Japan, Disaster Prevention Research Institute, Annals, **22**(B-2).

Whitham, G. B. 1999. *Linear and Nonlinear Waves*. Pure and applied mathematics. New York, *etc.*, John Wiley & Sons, Inc.

Zwinger, T., A. Kluwick and P. Sampl. 2003. Simulation of dry-snow avalanche flow over natural terrain. *In* Hutter, K. and N. Kirchner, *eds*. *Dynamic Response of Granular and Porous Materials under Large and Catastrophic Deformations, Lecture Notes in Applied and Computational Mechanics*. Heidelberg, Springer, **11**, 161–194.

A Summary of the dam design procedure

It is proposed that the design height of *both catching and deflecting dams* be determined based on essentially the *same dynamic principles* and carried out in a stepwise fashion according to the following list. The required dam height, H, normal to the terrain, is the sum of the run-up of the design avalanche on the dam side, h_r, and the snow depth on the terrain upstream of the dam, h_s,

$$H = h_r + h_s \ , \quad \text{where} \quad h_r = \max(H_{cr} + h_{cr}, h_2 + \Delta H_{\psi_\perp} + \Delta H_\kappa) \ . \tag{41}$$

The steps are as follows (see Figs. 1, 2, 3 and 4 and the list on page 54 below for explanations of the meaning of the variables):

1. Estimate appropriate design values for the velocity and flow depth of the avalanche at the location of the dam, u_1, h_1, and for the snow depth on the terrain upstream of the dam, h_s.

2. For a deflecting dam, determine the deflecting angle φ. For a catching dam, $\varphi = 90^\circ$.

3. Compute the Froude number of the flow, Fr, according to Equation (4), and the component of the velocity normal to the dam axis, $|u_\eta| = u_1 \sin\varphi$. Determine the momentum loss coefficient k according to Equation (27). The coefficient k represents the loss of momentum normal to the dam axis in the impact and depends on the angle of the upper dam side with respect to the terrain α.

4. Compute the sum of the critical dam height, H_{cr}, and the corresponding critical flow depth, h_{cr}, according to Equation (6) or (7) (see Fig. 5). The dam height above the snow cover must be greater than $H_{cr} + h_{cr}$. If the dam height above the snow cover is lower than H_{cr}, the avalanche may overflow the dam in a supercritical state. If the dam height is lower than $H_{cr} + h_{cr}$, the front of the avalanche may overflow the dam while a shock is being formed. Note that some overflow may occur in the initial impact due to splashing even when this criterion is satisfied.

5. Compute the flow depth, h_2, downstream of a shock upstream of the dam according to Equation (22) (see Fig. 7). The dam height above the snow cover, h_r, must also be greater than h_2.

6. The requirements expressed in the previous two items in the list are expressed graphically in Figure 15. The design dam height above the snow cover, $h_r = H - h_s$, corresponding to given values of h_1 and $|u_\eta|$, may be read directly from the higher one of the two curves on the graph (representing supercritical overflow and flow depth downstream of a shock, respectively).

7. For a *deflecting dam*, check whether an attached, stationary, oblique shock is dynamically possible by verifying that the deflecting angle, φ, is smaller than the maximum deflecting angle, $\varphi_{\max}$, corresponding to the Froude number Fr according to Equation (25) (see Fig. 8). It is recommended that φ is at least 10° smaller than $\varphi_{\max}$. If a dam does not satisfy this requirement, the flow depth downstream of the shock, h_2, in item 5 must be calculated for $\varphi = 90^\circ$. The dam is thus dimensioned as a catching dam with regard to the flow depth downstream of the shock, while the criterion based on supercritical overflow in item 4 is computed with the original value of φ as before.

8. If the terrain normal to the dam axis slopes towards the dam, the height of a *deflecting dam* derived from shock dynamics (see item 5) must be increased by $\Delta H_{\psi_\perp}$ according to Equation (31). The dam height corresponding to supercritical overflow ($H_{cr} + h_{cr}$, see item 4) is not increased due to this effect.

9. If the dam axis is curved, the height of a *deflecting dam* derived from shock dynamics (see item 5) must be increased by ΔH_κ according to Equation (32). This additional term may come on top of $\Delta H_{\psi_\perp}$ in case the upstream terrain slopes towards the dam as described in the previous item. The dam height corresponding to supercritical overflow ($H_{cr} + h_{cr}$, see item 4) is not increased due to this effect.

10. Compute the vertical dam height, H_D, by substituting r by H_D and h_r by H in Equation (37).

11. For a *deflecting dam*, evaluate the extent of the region affected by an *increased run-out distance* caused by the interaction of the avalanche with the dam. The construction of a dam leads to increased avalanche risk within this area. Also, evaluate the *lateral spreading of the avalanche downstream of the dam* (see Section 12). Possible lateral spreading will limit the area protected by the dam.

12. For a *catching dam*, compute the available storage space normal to the dam axis upstream of the dam per unit length along the dam according to Equation (34). The *storage per unit width* or *storage area*, S, must be larger than the volume of the avalanche divided by its width (see Fig. 18).

The main new features of this procedure to dimension dams are:

- The dam design is based on a *consistent dynamic description* of the interaction of shallow granular flow and an obstruction.

- *Shock dynamics* are used to derive run-up heights on dams, which determine the dam height under some conditions.

- The necessary dam height to prevent *supercritical overflow* is also used to derive run-up heights on dams, which determines the design-dam height under other conditions.

- A *maximum allowable deflecting angle*, derived from shock dynamics, limits the range of possible deflecting angles of deflecting dams.

- *Momentum loss in the impact with a dam* is calculated from the component of the velocity normal to the dam in the same way for both catching and deflecting dams.

- Avalanche flow along deflecting dams becomes *channelised*, which may lead to a substantial *increase in run-out* in the direction of the channelised flow.

- A consistent dynamic framework makes it possible to account for the *slope of the terrain* where a dam is located and a *curvature of the dam axis* in the dam design.

In practice, these requirements are satisfied in an iterative process, where the dam location, the slope of the upstream face of the dam and the deflecting angle are varied to minimise the construction cost, while taking into account other relevant conditions such as distance to the protected settlement, availability of suitable construction materials and various environmental aspects.

The above procedure is not applicable for wet-snow avalanches.

B Notation

The following list defines the variables used to describe the geometry of the terrain and the dam and the flow of the (dense core of the) avalanche at the dam location. Figures 1, 2 and 3 provide schematic illustrations of the meaning of the variables.

u_1, h_1 Velocity and flow depth of the oncoming flow upstream of any disturbance to the flow caused by the dam.

Fr Froude number, $\mathrm{Fr} = \frac{u}{\sqrt{g \cos\psi\, h_1}}$.

$\mathrm{Fr}_\perp$ "Froude number" corresponding to the component of the velocity normal to the dam, $\mathrm{Fr}_\perp = \mathrm{Fr} \sin\varphi$.

Fr_n "Froude number" corresponding to the component of the velocity normal to the shock in a moving frame of reference where the shock is stationary.

H Dam height. In this document, H is measured in the direction normal to the terrain in order to simplify derivations and formulations of results. In the final formulation of design criteria, dam height is defined in a vertical cross section normal to the dam axis in a horizontal plane.

$\Delta H_{\psi_\perp}$ Extra deflecting dam height due to terrain slope towards the dam.

ΔH_κ Extra deflecting dam height due to the effect of the curvature of the dam axis.

H_D Vertical dam height measured in a vertical cross section normal to the dam axis in a horizontal plane.

h_s Thickness of snow and previous avalanche deposits on the ground on the upstream side of the dam before an avalanche falls.

r Vertical run-up of an avalanche measured in a vertical section normal to a dam or obstacle axis in a horizontal plane.

H_{cr} Critical dam height. The maximum height of a dam over which uninterrupted, supercritical flow may be maintained.

h_{cr} Critical flow depth. Depth of flow over a dam with height H_{cr} at the top of the dam.

h_r Run-up height or design dam height, depending on the context, above the snow cover, $h_r = \max(H_{cr} + h_{cr}, h_2)$.

R_κ Radius of curvature of the dam axis.

u_2, h_2 Velocity and flow depth downstream of a shock that is formed in the flow against a dam.

S Storage space per unit width of the avalanche above a catching dam.

ψ Slope of the terrain at the location of the dam.

$\psi_\perp$ Slope of the terrain in the direction normal to the dam axis.

α Angle of the dam side with respect to the sloping terrain in the direction normal to the dam axis in a plane normal to the upstream terrain.

α_s The steepest inclination of the dam side.

φ Deflecting angle of the dam ($\varphi = 90^\circ$ for a catching dam) in a sloping coordinate system aligned with the terrain.

φ_h Deflecting angle of the dam ($\varphi_h = 90^\circ$ for a catching dam) in the map plane, that is the angle between the horizontal projections of the avalanche direction and the dam axis.

$\varphi_{\max}$ Maximum deflecting angle for which an attached, stationary, oblique shock may be formed.

φ_{lsp} Maximum lateral spreading (in terms of the angular width of the fan) beyond the dam axis formed at the downstream end of a deflecting dam.

θ Shock angle for a stationary, oblique shock upstream of a deflecting dam.

Δ Widening of a shock along a deflecting dam, $\Delta = \theta - \varphi$.

k Relative reduction in normal velocity in the impact with the dam.

λ An empirical parameter describing the effect of momentum loss during the impact and the effect of friction of the avalanche against the upstream side of the dam in the traditional expression for design dam height.

μ Friction coefficient for Coulomb friction.

ϕ Internal friction angle of avalanching snow.

x, y, z A coordinate system with the x,y-axes in the plane of the terrain near the dam location with the x-axis in the direction of the oncoming flow upstream of the dam.

ξ, η, ζ A coordinate system with the ξ,η-axes in the plane of the terrain near the dam location with the ξ-axis along the axis of the dam and the η-axis normal to the dam. ξ is also used to denote distance along the dam axis from the upstream end of a (possibly curved) deflecting dam.

u_ξ, u_η Velocity components parallel to the terrain in the ξ,η,ζ-system.

n, s A coordinate system moving with the shock with the s,n-axes in the plane of the terrain near the dam location with the s-axis in the direction of the shock formed above of the dam and the n-axis normal to the shock.

u_n, u_s Velocity components in the s,n-system ($u_s = 0$).

C The R package *viadam*

The formulas for the computation of supercritical run-up and flow depth downstream of a shock described in Sections 5 and 6 have been written up and documented as a library for the public doman software package R (see "http://www.r-project.org/" and "http://cran.r-project.org/"). R is a free software environment and programing language for statistical computing and graphics. It compiles and runs on a wide variety of UNIX platforms, Windows and MacOS. The `viadam` package includes functions to compute various characteristics of oblique shocks, the deflecting angle in a sloping reference frame aligned with the terrain, φ, from the deflecting angle in the map plane, φ_h, and vice versa, the vertical dam height H_D from dam height normal to the sloping terrain, H, and various other transformations and formulas that are described in Section 14. The package may be downloaded from the avalanche and landslide section of the web of Icelandic Meteorological Office ("http://www.vedur.is"). The documentation of this package is reproduced on the following pages.

Package 'viadam'

October 20, 2008

Title VI-Avalanche-Dams, height and geometry for avalanche dams

Version 1.0

Author Tomas Johannesson, Icelandic Met. Office

Description R-functions for computation of design height and geometry for avalanche dams, run-up height of avalanches on dams and natural obstructions and various other quantities related to the flow of snow avalanches against obstructions. The functions are bundled together in this package to provide a tested software package for evaluating expressions that are described in the report "The design of avalanche protection dams. Recent practical and theoretical developments" edited by Tomas Johannesson, Peter Gauer, Dieter Issler and Karstein Lied (Luxembourg, European Communities, 2008, ISBN 978-92-79-08885-8). Note that this software is only intended to assist an avalanche expert and does not replace the professional judgement of the user. No guaranty is provided that the software is free from errors or ambiguities. The user must verify computational results independently. All design decisions made with the assistance of this software are the responsibility of the user.

Maintainer Tomas Johannesson <tj@vedur.is>

License GPL2

R topics documented:

`damangle` *Angle of a dam side with respect to the surrounding terrain*

Description

Computes the angle of a dam side with respect to the sloping, upstream surrounding terrain from deflecting angle, slope of the terrain, and the steepest slope of the dam side.

Usage

```
damangle(phi,psi,alfas)
```

Arguments

`phi`	deflecting angle with respect to the direction of steepest decent in a sloping coordinate system aligned with the terrain.
`psi`	the slope of the terrain.
`alfas`	the steepest slope of the dam side.

Value

`damangle` returns a vector of angles subtended by the dam side with respect to the terrain with the same number of elements as `phi`, `psi` or `alfas`.

Note

The angle of the dam side with respect to the sloping terrain is measured in the direction normal to the dam axis in a plane normal to the upstream terrain.

The angles `phi`, `psi` and `alfas` are given in radians.

Author(s)

Tomas Johannesson

See Also

`vdamheight`, `sdamslope`, `phi2phi` and `phicontour`.

Examples

```
## Not run:
damangle(25*pi/180,10*pi/180,45*pi/180)
## End(Not run)
```

`mound.jump` *Geometry of a jet formed in the impact with a mound or a dam.*

Description

Compute the ballistic trajectory of a jet formed by the flow of an avalanche that hits a braking mound or a dam.

Usage

```
mound.jump(u0,beta,h,psi,k,fph=0.004,dt=0.1)
```

Arguments

`u0`	upstream velocity in metres per second.
`beta`	throw angle in the sloping coordinate system aligned with the terrain.
`h`	height of the mound above the snow cover in the direction normal to the terrain.
`psi`	slope of the terrain.
`k`	dimensionless number representing the effect of energy dissipation in the impact of the avalanche with the mound, recommended value is is `k` = 0.8, but `k` = 0.7, 0.8 and 0.9 should all be tested. The value of `k` is the throw velocity of the jet at the top of the dam relative to the velocity that corresponds to no loss of mechanical energy.
`fph`	a coefficient with dimensions of m^{-1} that represents the effect of air resistance on the jet, default value is 0.004 m^{-1}.
`dt`	time step in the Runge-Kutta integration, default value is 0.1 s.

Value

The function returns a list of vectors including the elements `res`, which contains the result of the integration: `u1` (throw speed from the top of the mound), `x2` (slope distance to the landing point of the jet), `x2cpsi` (map distance to the landing point of the jet), `u2` (speed of the jet at the landing point) and `betalnd` (angle of the jet at the landing point with respect of the terrain); `par`, which contains the arguments of the call to the function; and `x`, `y` and `u`, which are arrays of coordinates and speed along the computed trajectory.

Note

The computation of the ballistic jet is carried out in a sloping coordinate system that is aligned with the terrain in the neighbourhood of the mound or dam. This must be taken into consideration if one wishes to draw the geometry of the jet using the returned arrays `x` and `y` (`x` represents distance from the mound top along the sloping terrain and `y` is height above the terrain/snow cover in the direction normal to the terrain).

The height of the mound is defined as the height above the snow cover. The snow cover is for simplicity assumed to be uniform in thickness all along the terrain down to the landing point of the jet.

Author(s)

Tomas Johannesson

See Also

viadam.runge.kutta.

Examples

```
## Not run:
mound.jump(32,55*pi/180,10,11*pi/180,k=0.8)$res
## End(Not run)
```

---

mxphi *The maximum deflecting angle of an oblique shock*

Description

Computes the deflecting and shock angles corresponding to the maximum deflecting angle that separates the weak and strong oblique shocks for a particular value of the Froude number.

Usage

```
mxphi(Fr,method=c("exact","approximate"))
```

Arguments

Fr	Froude number.
method	method for the computation. For method = "exact", a numerical solution of the exact oblique shock relations is found. For method = "approximate", an approximate explicit solution valid for large Froude numbers is used.

Value

mxphi returns returns dataframe with two column: the shock angle teta) and the deflecting angle phi. They have the same number of elements as Fr.

Note

The returned angles teta and phi are given/returned in radians.

The approximate expression for the maximum deflecting angle, used when method = "approximate", is accurate to $O(Fr^{-5/2})$).

Author(s)

Tomas Johannesson

See Also

obliqueshock and obliquenshock.

Examples

```
## Not run:
mxphi(7,method="exact")
## End(Not run)
```

obliquenshock *Approximate characteristics of an oblique shock*

Description

Computes the shock angle, shock thickness, downstream velocity and downstream momentum flux for an oblique shock as functions of deflecting angle and Froude number using an approximation based on the flow against a normal shock with the speed of the normal component of the oblique flow.

Usage

```
obliquenshock(phi,Fr)
```

Arguments

phi	deflecting angle with respect to the direction of steepest decent in a sloping coordinate system aligned with the terrain.
Fr	Froude number.

Value

obliquenshock returns a dataframe containing the variables phi (deflecting angle), delta (difference between teta and phi, *i.e.* width of the stream along the deflecting wall), teta (shock angle), h2ph1 (relative change in flow depth across the shock), u2pu1 (relative change in flow speed across the shock) and h2u2ph1u1 (relative change in momentum flux across the shock). These variables have the same number of elements as teta or Fr. The Froude number and the Froude number normal to the wall are returned as the attributes Fr and Fp of the list.

Note

The angle phi is given in radians and so are all angles that are returned by the function.

This function computes the characteristics of a weak oblique shock. The corresponding strong oblique shock with a (much) larger value of the shock angle teta is eliminated by the approximations used in the derivations of the formulas used. The function obliqueshock may be used to obtain both types of the oblique shock.

The approximations used in this function provide good accuracy for Fr>2.5 and deflecting angles phi somewhat below the maximum deflecting angle which separates the weak and strong shocks for a particular value of the Froude number Fr.

Author(s)

Tomas Johannesson

See Also

obliqueshock and mxphi.

Examples

```
## Not run:
obliquenshock(15*pi/180,7)
## End(Not run)
```

`obliqueshock` *Characteristics of an oblique shock*

Description

Computes the deflecting angle, shock thickness, downstream velocity and downstream momentum flux for an oblique shock as functions of shock angle and Froude number.

Usage

```
obliqueshock(teta,Fr)
```

Arguments

`teta`	shock angle.
`Fr`	Froude number.

Value

`obliqueshock` returns a dataframe containing the variables `teta` (shock angle), `phi` (deflecting angle), `delta` (difference between `teta` and `phi`, *i.e.* width of the stream along the deflecting wall), `h2ph1` (relative change in flow depth across the shock), `u2pu1` (relative change in flow speed across the shock) and `h2u2ph1u1` (relative change in momentum flux across the shock). These variables have the same number of elements as `teta` or `Fr`. The Froude number is returned as the attribute `Fr` of the list.

Note

The angle `teta` is given in radians and so are all angles that are returned by the function.

This function returns the theoretically exact oblique shock solution, which represents both the weak and strong shocks, so that the shock angle `teta` is a double valued function of the deflecting angle `phi`.

Author(s)

Tomas Johannesson

See Also

`obliquenshock` and `mxphi`.

Examples

```
## Not run:
obliqueshock(22*pi/180,7)
## End(Not run)
```

phi2phi *Deflecting angles in different coordinate systems*

Description

Convert from a deflecting angle in a sloping coordinate system aligned with the terrain to deflecting angle in a horizontal projection.

Usage

```
phi2phi(phi,phih,psi)
```

Arguments

phi	deflecting angle with respect to the direction of steepest decent in a sloping coordinate system aligned with the terrain.
phih	deflecting angle with respect to the direction of steepest decent in the map plane, that is the angle between the horizontal projections of the avalanche direction and the dam axis.
psi	the slope of the terrain.

Value

phi2phi returns a vector of angles with the same number of elements as phi, phih or psi.

Note

The arguments must be named so that the routine can differentiate between phi and phih.

The angles phi, phih and psiare given in radians.

In general, phi $\leq$ phih so that the deflecting angle in the map plane may be used as a conservative estimate of the deflecting angle for dam design.

Author(s)

Tomas Johannesson

See Also

vdamheight, sdamslope, damangle and phicontour.

Examples

```
## Not run:
phi2phi(phi=25*pi/180,psi=10*pi/180)
## End(Not run)
```

phicontour *"Deflecting" angle of contour lines on a dam side*

Description

Computes the "deflecting angle" of contour lines on a dam side from deflecting angle, slope of the terrain, and the angle of the dam side with respect to the terrain.

Usage

```
phicontour(phi,psi,alfa)
```

Arguments

phi	deflecting angle with respect to the direction of steepest decent in a sloping coordinate system aligned with the terrain.
psi	the slope of the terrain.
alfa	the angle of the dam side with respect to the sloping terrain in the direction normal to the dam axis in a plane normal to the upstream terrain.

Value

phicontour returns a vector of angles with the same number of elements as phi, psi or alfa.

Note

The returned "deflecting angle" of the contour lines on the dam side is defined in the map plane.

This function is useful in an analysis of the flow of avalanches against natural obstructions where a "dam axis" is in many cases not easily defined. The returned "deflecting angle" of the contour lines may be compared with angles measured from maps and used to compute the deflecting angles phi and phih (see phi2phi) corresponding to a dam that is dynamically equivalent to the terrain obstruction.

The angles phi, psi and alfa are given in radians.

Author(s)

Tomas Johannesson

See Also

vdamheight, sdamslope, damangle and phi2phi.

Examples

```
## Not run:
phicontour(25*pi/180,10*pi/180,40*pi/180)
## End(Not run)
```

runuph *Run-up height of an avalanche on a dam or an obstacle.*

Description

Run-up height of an avalanche on a dam or an obstacle corresponding to both supercritical overflow and downstream thickness of a shock.

Usage

```
runuph(phih,u1,h1,psi,psip,alfa,k,kp,xi,hs)
```

Arguments

phih	deflecting angle with respect to the direction of steepest decent in the map plane, that is the angle between the horizontal projections of the avalanche direction and the dam axis.
u1	upstream velocity in metres per second.
h1	upstream flow depth in metres.
psi	the slope of the terrain.
psip	the slope of the terrain in the direction normal to the dam.
alfa	the angle of the dam side with respect to the sloping terrain in the direction normal to the dam axis in a plane normal to the upstream terrain.
k	a dimensionless coefficient representing momentum loss normal to the dam axis in the impact, computed from alfa if not specified.
kp	curvature of the dam axis for a deflecting dam, equal to one over the radius of curvature, set to zero if not specified.
xi	distance along the dam from its upstream end or the upstream end of the impact with the avalanche, set to zero if not specified.
hs	snow depth and thickness of previous avalanche deposits on the terrain, set to zero if not specified.

Value

The function returns a dataframe with variables/columns describing supercritical overflow and shock that may be formed by the upstream dam face. The variables of the returned dataframe are:

phi	deflecting angle with respect to the direction of steepest decent in a sloping coordinate system aligned with the terrain.
Fr1	upstream Froude number.
u1n	velocity normal to the dam axis.
Fr1n	"Froude number" in the direction normal to the dam axis.
Hcr	critical dam height.
hcr	critical flow depth.
hrp	supercritical run-up, *i.e.* H_{cr} + h_{cr}.

teta	shock angle.
delta	shock widening, *i.e.* the angle subtended by the shock with respect to the dam.
h2	flow depth downstream of a shock.
u2	flow velocity downstream of a shock.
dHslp	extra run-up due to slope towards the dam for a deflecting dam.
dHcrv	extra run-up due to dam curvature for a deflecting dam.
hrmx	maximum of supercritical run-up and flow depth downstream of a shock plus extra run-up due to slope towards the dam and dam curvature for a deflecting dam and plus snow depth on the terrain (in the sloping coordinate system aligned with the terrain).
hd	vertical runup corresponding to hrmx.

The attribute par of the returned variable contains the arguments of the call to the function, also as a dataframe.

Note

In contrast to most of the other functions in the viadam library, this function accepts dimensional arguments (*e.g.* flow depth in metres and velocity in metres per second) and returns dimensional quantities (*e.g.* dam height in metres). Most of the other functions accept non-dimensional quantities such as Froude numbers and angles and return non-dimensional quantities such as the downstream flow depth h_2 relative to the upstream flow depth h_1.

The arguments k, kp, xi and hs are optional and have default values that are described above. They should be named ef they are specified (see example with hs specified in the Examples section).

Author(s)

Tomas Johannesson

See Also

obliquenshock, mxphi and vdamheight.

Examples

```
## Not run:
runuph(18*pi/180,45,2,11*pi/180,3*pi/180,35*pi/180,hs=3)
## End(Not run)
```

---

sdamslope *Steepest slope of a dam side*

Description

Computes the steepest slope of a dam side from deflecting angle, slope of the terrain, and the angle of the dam side with respect to the terrain.

Usage

```
sdamslope(phi,psi,alfa)
```

Arguments

phi	deflecting angle with respect to the direction of steepest decent in a sloping coordinate system aligned with the terrain.
psi	the slope of the terrain.
alfa	the angle of the dam side with respect to the sloping terrain in the direction normal to the dam axis in a plane normal to the upstream terrain.

Value

sdamslope returns a vector of slopes with the same number of elements as phi, psi or alfa.

Note

The angles phi, psi and alfa are given in radians.

Author(s)

Tomas Johannesson

See Also

vdamheight, damangle, phi2phi and phicontour.

Examples

```
## Not run:
sdamslope(25*pi/180,10*pi/180,40*pi/180)
## End(Not run)
```

---

vdamheightngi *Vertical dam height with an alterative formula*

Description

Computes vertical dam height from dam height normal to the terrain, deflecting angle, slope of the terrain, and the angle of the dam side with respect to the terrain.

Usage

```
vdamheightngi(phi,psi,alfa,h)
```

Arguments

phi	deflecting angle with respect to the direction of steepest decent in a sloping coordinate system aligned with the terrain.
psi	the slope of the terrain.
alfa	the angle of the dam side with respect to the sloping terrain in the direction normal to the dam axis in a plane normal to the upstream terrain.
h	dam height normal to the terrain.

Value

vdamheightngi returns a vector of vertical dam heights with the same number of elements as phi, psi, alfa or h.

Note

The vertical dam height is measured in a vertical cross section normal to the dam or obstacle axis in the map plane.

The angles phi, psi and alfa are given in radians.

This function is equivalent to the function vdamheight but uses a different mathematical expression (from NGI reports) to compute the vertical damheight. It is only defined for validation purposes.

Author(s)

Tomas Johannesson

See Also

vdamheight.

Examples

```
## Not run:
vdamheightngi(25*pi/180,10*pi/180,40*pi/180,15)
## End(Not run)
```

---

vdamheight *Vertical dam height*

Description

Computes vertical dam height from dam height normal to the terrain, deflecting angle, slope of the terrain, and the angle of the dam side with respect to the terrain.

Usage

```
vdamheight(phi,psi,alfa,h)
```

Arguments

phi	deflecting angle with respect to the direction of steepest decent in a sloping coordinate system aligned with the terrain.
psi	the slope of the terrain.
alfa	the angle of the dam side with respect to the sloping terrain in the direction normal to the dam axis in a plane normal to the upstream terrain.
h	dam height normal to the terrain.

Value

vdamheight returns a vector of vertical dam heights with the same number of elements as phi, psi, alfa or h.

Note

The vertical dam height is measured in a vertical cross section normal to the dam or obstacle axis in the map plane.

The angles phi, psi and alfa are given in radians.

Author(s)

Tomas Johannesson

See Also

sdamslope, damangle, phi2phi, phicontour and vdamheightngi.

Examples

```
## Not run:
vdamheight(25*pi/180,10*pi/180,40*pi/180,15)
## End(Not run)
```

---

viadam.mxdffn *Utility function to compute the maximum deflecting angle as a function of shock angle*

Description

Computes an expression related to the the derivative of the deflecting angle as a function of the shock angle for use in a function to compute the maximum deflecting angle.

Usage

```
viadam.mxdffn(teta,Fr)
```

Arguments

teta	shock angle.
Fr	Froude number.

Value

viadam.mxdffn returns a vector of values of an expression related to the derivative of the deflecting angle phi as a function of the shock angle teta for the given value of the Froude number Fr. This expression is zero at the maximum deflecting angle for the given Froude number. The returned vector has the same number of elements as teta.

Note

The angle `teta` is given in radians and so is the returned angle `phi`.

This function is written for use in the function `mxphi` and is not intended for other use.

Author(s)

Tomas Johannesson

See Also

`mxphi`.

Examples

```
## Not run:
viadam.mxdffn(22*pi/180,7)
## End(Not run)
```

`viadam.runge.kutta` *Fourth-order Runge-Kutta integration*

Description

One step of the fourth-order Runge-Kutta integration algorithm for a first order system of differential equations.

Usage

```
viadam.runge.kutta(x,dx,y,f)
```

Arguments

`x`	the starting point of the integration.
`dx`	the step size in `x`.
`y`	the initial value of the solution at `x` (a vector of the same length as the number of equations).
`f`	a function expressing the derivative of `y` with respect to `x` as a function of `x` and `y`, that is the right hand side of the differential equation `y' = f(x,y)`. `f` must be defined as a function of two arguments (a single number `x` and a vector `y` of the same length as the number of equations) returning a vector (of the same length as the number of equations).

Value

The function returns the solution `y` at `x+dx`.

Note

`viadam.runge.kutta` is typically called repeatedly increasing the value of `x` by `dx` in every iteration as shown in the example. The argument `f` must be a function object, which can either be defined beforehand and referred to by its name, or be defined on the fly as in

`viadam.runge.kutta(x,dx,y,(function(x,y){y})).`

This function is written for use in the function `mound.jump` and is not intended for other use. It is included in the `viadam` package to make the package independent of any other utility package for R. There are many other packages that contain good Runge-Kutta integration routines that are more suitable for general use for solving differential equations. This routine is, however, good enough for the problem that needs to be solved in `mound.jump`.

Author(s)

Tomas Johannesson

See Also

`mound.jump`.

Examples

```
## Not run:
yp <- function(x,y) {c(y[2],y[1])}
n <- 10; dx <- 1/n; x <- 0; y <- c(1,1)
for (i in 1:n) { y <- viadam.runge.kutta(x,dx,y,yp); x <- x+dx }
y[1]
y[1]-exp(1)
## End(Not run)
```

Index